

# Stellar collisions in galactic centers: black hole growth and color gradients

Qingjuan Yu\*

*Princeton University Observatory, Peyton Hall, Princeton, NJ 08544-1001, USA*

24 December 2018

## ABSTRACT

We study the effects of stellar collisions, particularly on feeding massive black holes (BHs) and color gradients, in realistic galactic centers. We find that the mass released by stellar collisions is not sufficient to account for the present BH mass in galactic centers, especially in bright galaxies. This study, together with the study by Magorrian & Tremaine (1999) on tidal disruption of stars by massive BHs, implies that the material for BH growth (especially in galaxies brighter than  $\sim 10^9 L_\odot$ ) can only come from other sources, for example, the mass released by stellar evolution in the initial  $\sim 1$  Gyr of the galaxy’s lifetime, or the gas that sinks to the galactic center in a galaxy merger. We also analyze how the color of a stellar system is affected by collisions of stars. We find that collisions between main-sequence stars cannot cause observable color gradients in the visible bands at projected radius  $R \gtrsim 0.1''$  in M31, M32 and other nearby galactic centers. This result is consistent with the lack of an observable color gradient in M32 at  $R \gtrsim 0.1''$ . At even smaller radii, the color differences caused by collisions between main-sequence stars are at most 0.08 mag at  $R = 0.02''$ . The averaged blueing due to stellar collisions in the region  $R < 0.1''$  of M32 should not be larger than 0.06 mag in color index  $U - V$  and 0.02 mag in  $V - I$ . The observed blueing in the center of the galaxy M31 (in a  $0.14'' \times 0.14''$  box) must be caused by some mechanism other than collisions between main-sequence stars.

**Key words:** black hole physics – galaxies: individual: M31, M32 – galaxies: kinematics and dynamics – galaxies: photometry – galaxies: nuclei – stars: blue stragglers

## 1 INTRODUCTION

The centers of galaxies are extreme astrophysical environments. They house massive black holes (BHs) (e.g., Magorrian et al. 1998) and also densely packed stars ( $10^2\text{--}10^4 M_\odot \text{pc}^{-3}$  at galactic radius  $\sim 10$  pc, e.g., Faber et al. 1997). High stellar densities lead to frequent stellar collisions. The outcome of the collision between two stars depends on their types (e.g., evolutionary phase, mass and radius) and their kinematic parameters (e.g., relative velocity and impact parameter) (e.g., Freitag & Benz 2002). The two stars may both survive their collision, or the collision may destroy one or both of them, or lead to their coalescence. Gas released from the colliding stars may be accreted onto the central BH, and this process has been proposed as one of the contributions to growth of central massive BHs (e.g., Frank 1978). Coalesced stars may appear as new stars with different luminosity properties or different colors from their parents; thus the luminosity and color of galactic centers are possibly affected by stellar collisions. The purpose of this paper is to study the effects of stellar collisions, particularly on feeding BHs and color gradients, in realistic galactic centers.

Studies of central BHs in nearby galaxies have revealed a tight correlation between central BH mass and galactic velocity dispersion (e.g., Tremaine et al. 2002 and references therein), which strongly suggests a close link between the formation and evolution of galaxies and their central BHs. In an isolated stellar system, central BHs may accrete stellar mass from the following three sources: (i) gas released by tidal disruption of stars and stars swallowed whole by central BHs (mostly for

\* Present address: Canadian Institute for Theoretical Astrophysics, 60 St. George Street, Toronto, Ontario M5S 3H8, Canada, yuqj@cita.utoronto.ca

stars on elongated radial orbits which may come close to central BHs), (ii) gas released by stellar collisions, (iii) and gas lost by stellar winds. Whether the above three sources are sufficient to account for the present BH mass and which is the main contributor to the BH growth depend on the stellar density distribution and velocity dispersion (e.g., Duncan & Shapiro 1983; Murphy, Cohn & Durisen 1991; Freitag & Benz 2002). The first source in this list, tidal disruption of stars, has been studied by Magorrian & Tremaine (1999). They show that the total mass of stars that are tidally disrupted or swallowed whole over the lifetime of typical nearby galaxies is of the order of  $10^6 M_\odot$ , approximately independent of galaxy luminosity. Thus disrupted stars may contribute significantly to the present BH mass only in faint galaxies ( $\lesssim 10^9 L_\odot$ ). One part of this paper (§ 3) studies whether the second source (i.e., gas released by stellar collisions) is sufficient to explain current BH masses in realistic galactic centers.

The colors of galactic centers reflect the constituents of their stellar population, and radial color gradients may provide much information on the formation and evolution of the stellar populations or galaxies. In § 4, we will analyze how the color of a stellar system is affected by collisions of main-sequence stars. We will focus on studying two galaxies in the Local Group: M31 and M32, which are the nearest giant spiral and dwarf elliptical galaxy (distance:  $\sim 800$  kpc) and have high-resolution observations of their centers in several color bands (Lauer et al. 1998). Multicolor *HST* WFPC2 (Wide Field Planetary Camera 2) images show that the center of M31 (the region within  $\sim 1$  pc of its central BH) appears bluer than the rest of nucleus and the surrounding bulge. Lauer et al. (1998) suggest that this blueing is caused by collisions between main-sequence stars since coalescence of main-sequence stars by collisions may form blue stragglers (which are brighter and bluer than their parent stars, e.g., Leonard 1989; Baily & Pinsonneault 1995). However, observations show that the center of M32 lacks color gradients at similar spatial resolution. The lack of color gradients in M32 is inconsistent with a rough estimate of the effects of collisions between main-sequence stars by Lauer et al. (1998), and this inconsistency is claimed to be an important puzzle. In § 4, we will study whether collisions of main-sequence stars can cause observable color gradients in the centers of M31, M32 and some other nearby galaxies.

Finally, our conclusions are given in § 5.

## 2 STELLAR COLLISION RATES AND TIMESCALES

We first present a general description of stellar collision rates and timescales.

In a stellar system, the distribution function (DF)  $f(\mathbf{x}, \mathbf{v})$  is defined so that  $f(\mathbf{x}, \mathbf{v}) d^3\mathbf{x}d^3\mathbf{v}$  is the number of stars within a phase-space volume  $d^3\mathbf{x}d^3\mathbf{v}$  of  $(\mathbf{x}, \mathbf{v})$ . We define the stellar mass function of the system at time  $t$  as  $\Xi(m, t)$ , so that  $\Xi(m, t) dm$  is the probability of finding a star with mass in the range  $m \rightarrow m + dm$  (i.e.,  $\int_0^\infty \Xi(m, t) dm = 1$ ); and we define the stellar mass and radius function at time  $t$  as  $\xi(m, a, t)$ , so that  $\xi(m, a, t) dm da$  is the probability of finding a star with mass and radius in the range  $(m, a) \rightarrow (m + dm, a + da)$  [i.e.,  $\int_0^\infty \xi(m, a, t) da = \Xi(m, t)$ ]. We assume that the stellar mass and radius function is independent of the location of the stars in the phase space  $(\mathbf{x}, \mathbf{v})$ .

The cross section for a physical collision (or contact encounter) of two stars with mass and radius  $(m_i, a_i)$  and  $(m_j, a_j)$  moving with the relative velocity at infinity  $v_{\text{rel}}$  is given by:

$$\Sigma_{ij}(v_{\text{rel}}) = \pi b^2 = \pi r_p^2 \left( 1 + \frac{v_{ij}^2}{v_{\text{rel}}^2} \right) \simeq \begin{cases} \pi r_p^2 & \text{if } v_{\text{rel}} \gg v_{ij} \\ \pi r_p^2 v_{ij}^2 / v_{\text{rel}}^2 & \text{if } v_{\text{rel}} \ll v_{ij} \end{cases}, \quad (1)$$

where  $b$  is the impact parameter,  $r_p = a_i + a_j$ , and  $v_{ij} = \sqrt{2G(m_i + m_j)/r_p}$ . If  $(m_i, a_i) = (m_j, a_j)$ ,  $v_{ij} = \sqrt{2Gm_i/a_i} \equiv v_{\text{esc}}$  is the escape velocity from the surface of either star. Thus, a star  $(m_j, a_j)$  moving with velocity  $\mathbf{v}_j$  through a background of stars with distribution function  $f(\mathbf{r}, \mathbf{v})$ , suffers collisions with stars with mass and radius in the range  $(m_i, a_i) \rightarrow (m_i + dm_i, a_i + da_i)$  at a rate  $\Gamma_{ij}(\mathbf{r}, \mathbf{v}_j) dm_i da_i$  given by (cf., eq. 8-116 in Binney & Tremaine 1987):

$$\Gamma_{ij}(\mathbf{r}, \mathbf{v}_j, t) dm_i da_i = \xi(m_i, a_i, t) dm_i da_i \int d^3\mathbf{v}_i f(\mathbf{r}, \mathbf{v}_i) |\mathbf{v}_i - \mathbf{v}_j| \Sigma_{ij}(|\mathbf{v}_i - \mathbf{v}_j|). \quad (2)$$

If the distribution of field stars is isotropic in velocity space, we set  $v = |\mathbf{v}|$  and we have

$$\Gamma_{ij}(\mathbf{r}, \mathbf{v}_j, t) dm_i da_i = \xi(m_i, a_i, t) dm_i da_i \int_0^\infty dv_i \frac{2\pi v_i}{v_j} f(\mathbf{r}, v_i) \int_{|v_i - v_j|}^{v_i + v_j} dv_{\text{rel}} v_{\text{rel}}^2 \Sigma_{ij}(v_{\text{rel}}). \quad (3)$$

The number of collisions between two stars with masses and radii in the ranges  $(m_i, a_i) \rightarrow (m_i + dm_i, a_i + da_i)$  and  $(m_j, a_j) \rightarrow (m_j + dm_j, a_j + da_j)$  per unit volume per unit time,  $\mathcal{R}_{ij}(\mathbf{r}) dm_i da_i dm_j da_j$ , is given by:

$$\mathcal{R}_{ij}(\mathbf{r}, t) dm_i da_i dm_j da_j = \xi(m_j, a_j, t) dm_j da_j \int d^3\mathbf{v}_j f(\mathbf{r}, \mathbf{v}_j) \Gamma_{ij}(\mathbf{r}, \mathbf{v}_j, t), \quad (4)$$

and we have  $\mathcal{R}_{ij} = \mathcal{R}_{ji}$ . We define the collision timescale of the stars with mass and radius  $(m_i, a_i)$  as follows:

$$t_{\text{coll},i}(\mathbf{r}, t) \equiv \frac{\xi(m_i, a_i, t) n(\mathbf{r}, t)}{\int dm_j da_j \mathcal{R}_{ji}(\mathbf{r}, t)}, \quad (5)$$

where  $n(\mathbf{r}, t) \equiv \int d^3\mathbf{v} f(\mathbf{r}, \mathbf{v})$  is the stellar number density at position  $\mathbf{r}$  and time  $t$ . Thus the total number density of the stars with mass and radius in the range  $(m_i, a_i) \rightarrow (m_i + dm_i, a_i + da_i)$  per unit time undergoing collisions is given by  $n(\mathbf{r}, t)\xi(m_i, a_i, t)dm_ida_i/t_{\text{coll},i}(\mathbf{r}, t)$ . For the whole stellar population, the collision timescale  $t_{\text{coll}}(\mathbf{r})$  is defined by:

$$t_{\text{coll}}(\mathbf{r}, t) \equiv \frac{n(\mathbf{r}, t)}{\int dm_ida_idm_jda_j \mathcal{R}_{ij}(\mathbf{r}, t)} = \frac{1}{\int dm_ida_i \xi(m_i, a_i, t)/t_{\text{coll},i}(\mathbf{r}, t)}, \quad (6)$$

and the total number of stars per unit time undergoing collisions is given by:

$$\dot{N}_{\text{coll}}(t) = \int d^3\mathbf{r} \frac{n(\mathbf{r}, t)}{t_{\text{coll}}(\mathbf{r}, t)}. \quad (7)$$

Note that stellar collision rates depend on the position  $\mathbf{r}$  in the stellar system and hence vary during the stellar orbit (unless the orbit is circular).

### 3 FEEDING CENTRAL MASSIVE BHS BY STELLAR COLLISIONS

In this section, we will study whether the mass released by stellar collisions makes a significant contribution to the growth of massive BHs in galactic centers.

#### 3.1 Stellar mass involved in collisions

The mass of gas released by two colliding stars depends on their relative velocity and impact parameter, as well as their masses and radii and their evolutionary phases (e.g., main-sequence stage or post-main-sequence stage) (e.g., Murphy, Cohn & Durisen 1991; Bailey & Davies 1999; Freitag & Benz 2002). We define  $\Delta m_{ij}(\mathbf{r})$  as the average gas mass released per collision between two stars with masses and radii  $(m_i, a_i)$  and  $(m_j, a_j)$  at position  $\mathbf{r}$ . The total gas mass released by stellar collisions per unit volume per unit time is given by:

$$\dot{\rho}_{\text{coll}}(\mathbf{r}, t) = \frac{1}{2} \int dm_ida_idm_jda_j \mathcal{R}_{ij}(\mathbf{r}, t) \Delta m_{ij}(\mathbf{r}), \quad (8)$$

where the collision rate  $\mathcal{R}_{ij}(\mathbf{r}, t)$  can be obtained from equation (4) and we have the factor “1/2” in front of the integration because the gas released from each colliding star is counted twice in the integration. The total collisionally released mass per unit volume at position  $\mathbf{r}$  until time  $t$  is given by  $\rho_{\text{coll}}(\mathbf{r}, t) = \int_0^t \dot{\rho}_{\text{coll}}(\mathbf{r}, t') dt'$ , and the total collisionally released mass over the age of the stellar system  $T_{\text{age}}$  is given by:

$$M_{\text{coll}}(T_{\text{age}}) = \int d^3\mathbf{r} \rho_{\text{coll}}(\mathbf{r}, T_{\text{age}}). \quad (9)$$

If all the released gas is accreted onto the central BH, equation (9) gives the mass growth of the central BH caused by stellar collisions. If  $\Delta m_{ij} = m_i + m_j$ , equation (9) gives the stellar mass involved or maximum gas mass released in collisions,  $M_{\text{coll}}^{\text{max}}(T_{\text{age}})$ .

To estimate an upper limit on the BH mass growth caused by stellar collisions, we will assume below that all the mass involved in collisions is released as gas and accreted onto the central BH. According to equation (6), the variation of the stellar number density is given by

$$\dot{n}(\mathbf{r}, t) = -n(\mathbf{r}, t)/t_{\text{coll}}(\mathbf{r}, t). \quad (10)$$

In equation (10), we have assumed that the stellar density at a position  $\mathbf{r}$  is affected only by collisions occurring near  $\mathbf{r}$ , and we will see in § 3.3 that our conclusions will not be significantly affected after relaxing this assumption. Now, we assume that the stars in the stellar system have a single mass  $m_*$  and a single radius  $a_*$  [i.e.,  $\xi(m, a, t) = \delta(m - m_*)\delta(a - a_*)$ , where  $\delta(x)$  is the Dirac function] and the stellar system initially has an isothermal distribution  $f(\mathbf{r}, \mathbf{v}) = n(\mathbf{r}, 0) \exp(-|\mathbf{v}|^2/2\sigma^2)/(2\pi\sigma^2)^{3/2}$  (where  $\sigma$  is the one-dimensional velocity dispersion). The initial collision timescale in this stellar system, which can be derived from equations (1)–(6), is given by (see also eq. 20 in Duncan & Shapiro 1983):

$$t_{\text{coll}}(\mathbf{r}, 0) = \frac{1}{16\sqrt{\pi}n(\mathbf{r}, 0)a_*^2\sigma[1 + v_{\text{esc}}^2/(4\sigma^2)]}. \quad (11)$$

In such a stellar system, if we ignore star formation, stellar evolution, gradual mass segregation or other evolutionary effects, then according to equation (6) [i.e.,  $t_{\text{coll}}(\mathbf{r}, t) \propto 1/n(\mathbf{r}, t)$ ] and equation (10), we find the stellar number density at time  $t$  given by:

$$n(\mathbf{r}, t) = \frac{n(\mathbf{r}, 0)}{1 + t/t_{\text{coll}}(\mathbf{r}, 0)}, \quad (12)$$

and the stellar collision timescale is given by  $t_{\text{coll}}(\mathbf{r}, t) = t + t_{\text{coll}}(\mathbf{r}, 0)$ . Thus, in the region where the initial collision timescale is much longer than the age of the stellar system [i.e.,  $t_{\text{coll}}(\mathbf{r}, 0) \gg T_{\text{age}}$ ], we have  $n(\mathbf{r}, T_{\text{age}}) \simeq n(\mathbf{r}, 0)$  (i.e., the stellar number density is affected little by collisions) and the collision timescale  $t_{\text{coll}}(\mathbf{r}, T_{\text{age}}) \simeq t_{\text{coll}}(\mathbf{r}, 0)$ ; while, in the region with  $t_{\text{coll}}(\mathbf{r}, 0) \ll T_{\text{age}}$ , we have  $n(\mathbf{r}, T_{\text{age}}) \simeq n(\mathbf{r}, 0)t_{\text{coll}}(\mathbf{r}, 0)/T_{\text{age}} \ll n(\mathbf{r}, 0)$  (i.e., stars are disrupted quickly by stellar collisions) and the collision timescale is  $t_{\text{coll}}(\mathbf{r}, T_{\text{age}}) \simeq T_{\text{age}}$ . The total gas mass released by collisions (or the upper limit of the total stellar mass involved in collisions) per unit volume over the age of the stellar system is given by:

$$\begin{aligned} \rho_{\text{coll}}^{\text{max}}(\mathbf{r}, t = T_{\text{age}}) &= m_* [n(\mathbf{r}, 0) - n(\mathbf{r}, T_{\text{age}})] \\ &\simeq \begin{cases} m_* n(\mathbf{r}, 0) T_{\text{age}} / t_{\text{coll}}(\mathbf{r}, 0) & \text{if } t_{\text{coll}}(\mathbf{r}, 0) \gg T_{\text{age}} \\ m_* n(\mathbf{r}, 0) & \text{if } t_{\text{coll}}(\mathbf{r}, 0) \ll T_{\text{age}} \end{cases}, \end{aligned} \quad (13)$$

and the total mass involved in stellar collisions over time  $T_{\text{age}}$  is given by:

$$M_{\text{coll}}^{\text{max}}(T_{\text{age}}) = \int d\mathbf{r}^3 \rho_{\text{coll}}^{\text{max}}(\mathbf{r}, T_{\text{age}}) \quad (14)$$

If the initial stellar density is singular, that is,

$$n(r, 0) = \frac{\sigma^2}{2\pi G m_* r^2} \quad (15)$$

(cf., eq. 4-123 in Binney & Tremaine 1987), then using equations (11)–(15), we have the total mass involved in stellar collisions over time  $T_{\text{age}}$  as follows:

$$M_{\text{coll}}^{\text{max}}(T_{\text{age}}) = \sqrt{A} \sigma^2 / G, \quad (16)$$

where

$$A = \frac{8\pi^{3/2} \sigma^3 a_*^2 T_{\text{age}}}{G m_*} \left( 1 + \frac{v_{\text{esc}}^2}{4\sigma^2} \right). \quad (17)$$

In a stellar system with a distribution of stellar masses and radii, if we ignore star formation, stellar evolution, gradual mass segregation or other evolutionary effects and we assume that collision timescales of stars with any given mass and radius ( $m_i, a_i$ ) do not change with time, i.e.,  $t_{\text{coll},i}(r, t) = t_{\text{coll},i}(r, 0)$ , we may obtain the number density of stars with mass and radius ( $m_i, a_i$ ) at time  $t$  is  $\Xi(m_i, 0)n(r, 0)e^{-t/t_{\text{coll},i}(r, 0)}$  (cf., eq. 10), and the stellar mass involved in collisions over the age of the stellar system is given as follows:

$$M_{\text{coll}}^{\text{max}}(T_{\text{age}}) = \int 4\pi r^2 dr \int dm_i m_i \Xi(m_i, 0) n(r, 0) [1 - e^{-T_{\text{age}}/t_{\text{coll},i}(r, 0)}]. \quad (18)$$

In reality, the collision timescale  $t_{\text{coll},i}(r, t)$  is not a constant and should increase with time,  $M_{\text{coll}}^{\text{max}}(T_{\text{age}})$  obtained from equation (18) is an upper limit to the stellar mass involved in collisions.

Ignoring star formation and stellar evolution in the study is usually a reasonable assumption for an old stellar system after the initial rapid stellar evolution of  $\sim 1$  Gyr is complete (i.e., massive stars have evolved into stellar remnants and the main-sequence stars have low masses with long lifetime and little change in the mass and radius in the main-sequence phase; cf., § 3.4). Stellar remnants of massive stars (BHs and neutron stars) may migrate inwards as a result of energy equipartition with low-mass field stars (e.g., Morris 1993), i.e., mass segregation. As will be discussed at the end of § 3.4, mass segregation affects little on our result of  $M_{\text{coll}}^{\text{max}}$  in most galactic centers, especially for bright galaxies.

### 3.2 Galaxy samples

In the past several years, images from the *Hubble Space Telescope (HST)* have revealed many details about the central regions of nearby galaxies, with a resolution of  $0.1''$ , corresponding to distances of  $\lesssim 10$  pc or  $\sim 10^6 (M_\bullet / 10^8 M_\odot)$  Schwarzschild radii for typical target galaxies (Byun et al. 1996). The inner surface brightness profiles of the galaxies as a function of projected radius  $R$  are well fitted with a five-parameter fitting function — the Nuker law (Faber et al. 1997):

$$I(R) = 2 \frac{\beta - \gamma}{\alpha} I_b \left( \frac{R}{r_b} \right)^{-\gamma} \left[ 1 + \left( \frac{R}{r_b} \right)^\alpha \right]^{-\frac{\beta - \gamma}{\alpha}}. \quad (19)$$

The asymptotic logarithmic slope inside  $r_b$  is  $-\gamma$ , the asymptotic outer slope is  $-\beta$ , and the parameter  $\alpha$  characterizes the sharpness of the break. The break radius  $r_b$  is the point of maximum curvature in log-log coordinates. The “break surface brightness”  $I_b$  is the surface brightness at  $r_b$ . According to the inner surface brightness profiles  $I(R) \propto R^{-\gamma}$  ( $r \rightarrow 0$ ), elliptical and spiral bulges (hot galaxies) can be classified into two types: core galaxies ( $\gamma \lesssim 0.3$ ) and power-law galaxies ( $\gamma \gtrsim 0.5$ ). A sample of nearby hot galaxies (elliptical galaxies or spiral bulges) observed by *HST* is collected in Faber et al. (1997), who estimate the stellar mass-to-light ratio  $\Upsilon$  (constant for each galaxy, determined by normalizing to the central velocity

dispersion based on spherical and isotropic models fitted to the Nuker-law profile) and the half-light radius (cf., Table 1 in Yu 2002). Assuming that the galaxies are spherical and isotropic (the mean ellipticity is 0.26), we may obtain their stellar density and velocity distributions by using the Eddington formula (eq. 4-140a in Binney & Tremaine 1987) and estimate their central BH masses  $M_\bullet$  by using the following relation between BH mass and galactic velocity dispersion (Tremaine et al. 2002)

$$\log(M_\bullet/M_\odot) = (8.13 \pm 0.06) + (4.02 \pm 0.32) \log(\sigma_e/200 \text{ km s}^{-1}), \quad (20)$$

where  $\sigma_e$  is the luminosity-weighted line-of-sight velocity dispersion inside the half-light radius. Note that the surface brightness profiles obtained in Faber et al. (1997) are based on *HST* WFPC1 data. We have updated the surface brightness profile of M32 using WFPC2 data in this paper (for detailed information, see § 4.2 or Lauer et al. 1998). In total, 31 galaxies from the Faber et al. sample will be used in this paper to study the effects of stellar collisions in galactic centers.

### 3.3 Results for simple stellar systems with identical stars

In this subsection, we use equation (6) to find the collision timescales as a function of galactic radius in realistic galactic centers (cf., § 3.2). The results are shown in Figure 1. Then, we will use equations (8)–(17) to obtain the stellar mass involved in collisions or the upper limit of mass released by collisions ( $M_{\text{coll}}^{\text{max}}$ ) over the Hubble time  $t_{\text{Hubble}} \simeq 10^{10}$  yr, which is shown in Figure 3. In this subsection, all the stars are assumed to have identical mass and radius and stellar evolution is ignored. In the next subsection, we will see that the generalization to a distribution of masses and radii will not significantly affect our conclusions.

Figure 1 shows the collision timescales  $t_{\text{coll},\odot}(r)$  as a function of radius  $r$  (the subscript “ $\odot$ ” indicates that the results are obtained by assuming that all stars have the solar mass and radius). The stellar distribution  $n(r)$  and the collision timescale  $t_{\text{coll},\odot}(r)$  within the region not resolved by the *HST* ( $2r < 0.1''$ ) are obtained by extrapolating the observed surface brightness profile (eq. 19) inward [i.e., assuming  $I(R) \propto R^{-\gamma}$  at  $2R < 0.1''$ ]. As seen from Figure 1, the collision timescales  $t_{\text{coll},\odot}(r)$  increase with increasing radius  $r$ . At radii  $r \gtrsim 0.003$ –1 pc (Fig. 1a), the collision timescales are longer than the Hubble time and the stellar distributions are affected little by stellar collisions [i.e.,  $n(\mathbf{r}, 0) \simeq n(\mathbf{r}, t_{\text{Hubble}})$  and  $t_{\text{coll}}(\mathbf{r}, 0) \simeq t_{\text{coll}}(\mathbf{r}, t_{\text{Hubble}})$ ], which is also true in the region resolved by *HST* ( $2r > 0.1''$ , cf., Fig. 1b). Figure 1(c) shows that in all galaxies, the region with  $t_{\text{coll},\odot}(r) < t_{\text{Hubble}}$  is located within the radius of the sphere of influence of the BH  $r_{\text{H}}$ , which is defined in terms of the intrinsic one-dimensional velocity dispersions of the galaxy  $\sigma(r)$  through

$$\sigma^2(r_{\text{H}}) \equiv GM_\bullet/r_{\text{H}}. \quad (21)$$

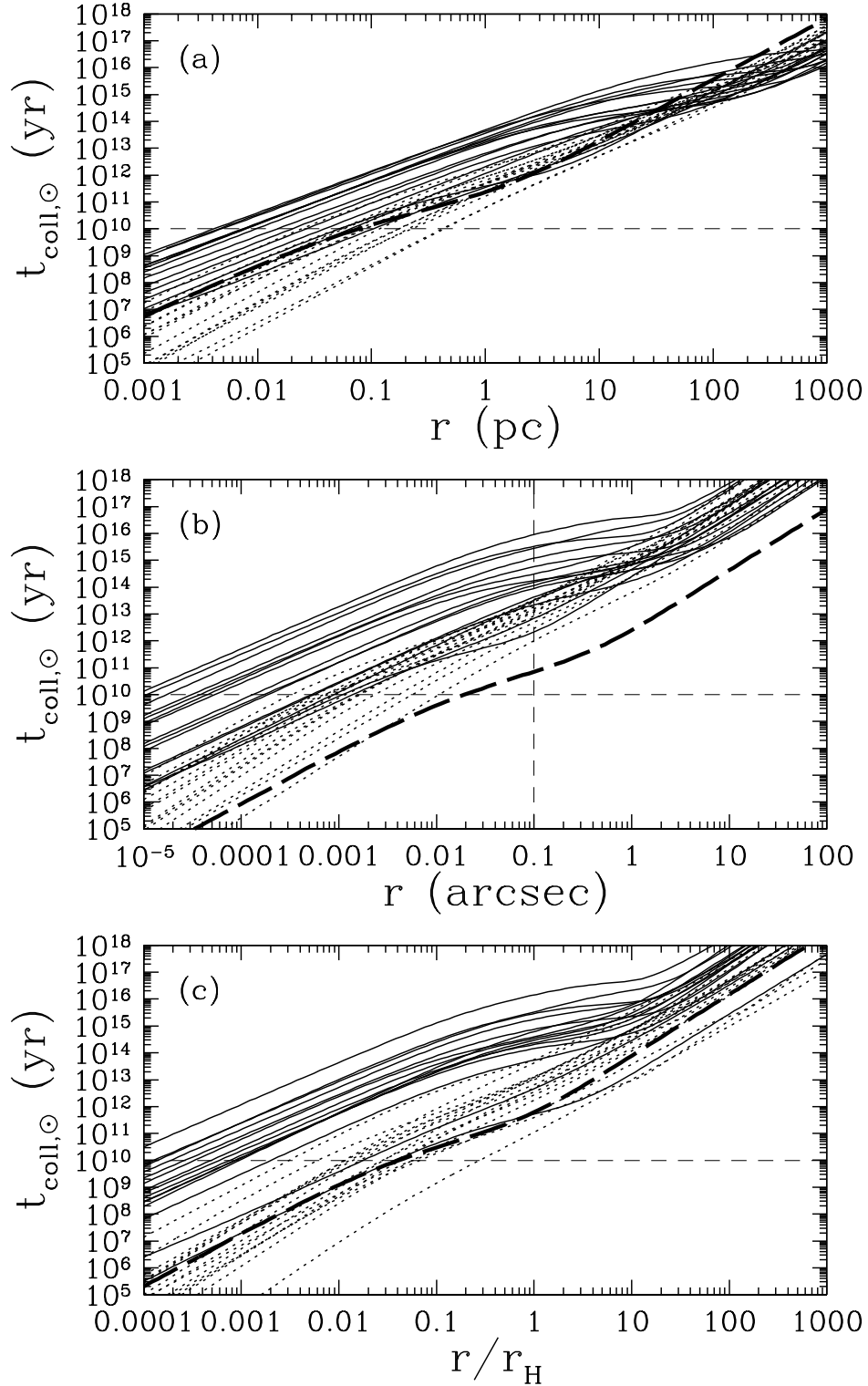
In the region where most stars should have been disrupted quickly [i.e.,  $t_{\text{coll},\odot}(r) \ll t_{\text{Hubble}}$ ], the stellar distribution obtained by extrapolating the Nuker law inward can only be interpreted as the initial stellar distribution and the corresponding collision timescales  $t_{\text{coll},\odot}(r)$  shown in Figure 1 are the initial collision timescales  $t_{\text{coll},\odot}(r, 0)$ . Current stellar densities in those regions may be estimated from equation (12), and current collision timescales are about  $t_{\text{coll}}(r, t_{\text{Hubble}}) \simeq t_{\text{Hubble}}$ .

Figure 2 shows the collision timescale  $t_{\text{coll},\odot}$  as a function of the ratio  $2\sigma(r)/v_{\text{esc},\odot}$ , where  $v_{\text{esc},\odot}$  is the escape velocity from stars with solar mass and radius (cf., eq. 1). As seen from Figure 2, the one-dimensional velocity dispersion  $\sigma(r)$  is not a monotonic function of  $t_{\text{coll},\odot}(r)$  or  $r$  (note that  $t_{\text{coll},\odot}$  is a monotonic increasing function of  $r$  in Fig. 1), which is due to the effect of central BHs. In the absence of central BHs, the velocity dispersion  $\sigma(r)$  should decrease with decreasing radius  $r$  at small  $r$  (cf., eq. 10 for case  $1 < \eta < 2$  in Tremaine et al. 1994); but with a central BH, the velocity dispersion increases with decreasing  $r$  at  $r \ll r_{\text{H}}$  [i.e.  $\sigma(r) \propto r^{-1/2}$ ]. Thus, with decreasing  $r$  or  $t_{\text{coll},\odot}(r)$ , the velocity dispersion  $\sigma(r)$  may show a minimum near the region where the effect of central BHs becomes dominant. Figure 2 shows that for all the core galaxies, the collision time is less than the Hubble time only if the velocity dispersion exceeds the escape speed.

Figure 3(a) shows the central BH mass  $M_\bullet$  versus the upper limit of the mass released by stellar collisions over a Hubble time  $M_{\text{coll},\odot}^{\text{max}}(t_{\text{Hubble}})$  (eq. 9) in the galaxies in our sample (open circles and solid circles). Once again, all stars are assumed to have the solar mass and radius. As seen from Figure 3(a), the upper limit of the mass released by stellar collisions over a Hubble time  $M_{\text{coll},\odot}^{\text{max}}(t_{\text{Hubble}})$  is smaller than the BH mass  $M_\bullet$  in *all* the galaxies of the sample. For power-law galaxies ( $M_\bullet \sim 10^5$ – $10^9 M_\odot$ , open circles),  $M_{\text{coll},\odot}^{\text{max}}$  is usually in the range  $\sim 10^4$ – $10^7 M_\odot$ ; and for core galaxies ( $M_\bullet \sim 10^8$ – $10^9 M_\odot$ , solid circles),  $M_{\text{coll},\odot}^{\text{max}} \sim 10^4$ – $10^6 M_\odot$ . Thus, other material sources, rather than mass released by stellar collisions, must dominate the growth of central BHs, especially in core galaxies. In Figure 3(a), we also show the results obtained from simplified galaxy models with Maxwellian stellar distributions with dispersion independent of radius (dashed lines). The short dashed lines are obtained by assuming that the galaxies have flat inner stellar densities (see eqs. 4-124b and 4-128a in Binney & Tremaine 1987)

$$n(r) = n_c/[1 + (r/r_c)^2]^{3/2}, \quad (22)$$

where  $n_c = 9\sigma^2/(4\pi Gm_*r_c^2)$ . The core radius  $r_c$  is set to be in the range  $10^2$ – $10^3$  pc. Note that it is only in the singular case that the density in equation (15) and a Maxwellian velocity distribution are an exact solution of the collisionless Boltzmann equation. The long dashed line is obtained by assuming that the galaxies have singular stellar densities (see eqs. 15–17).



**Figure 1.** Stellar collision timescales as a function of galactic radius (eq. 6). The galaxy sample comes from Table 1 in Yu (2002). Stars are assumed to all have the solar mass and radius. In the region not resolved by the *HST* ( $2r < 0.1''$ ), the collision timescales are obtained by extrapolating the surface brightness profiles (eq. 19) inward. The solid curves represent core galaxies ( $\gamma \leq 0.3$ ) and the dotted curves represent power-law galaxies ( $\gamma \geq 0.5$ ). The thick dashed line represents the galaxy M32, whose central colors will be studied in detail in § 4.2. The three panels use three different measures of radius: parsecs, arcsec and  $r_H$ , where  $r_H$  is the radius of the sphere of influence of the BH, defined implicitly in terms of the intrinsic one-dimensional velocity dispersion of the galaxy  $\sigma(r)$  through equation (21). For how the results shown in this Figure are affected after generalizing to a distribution of masses and radii, see § 3.4.

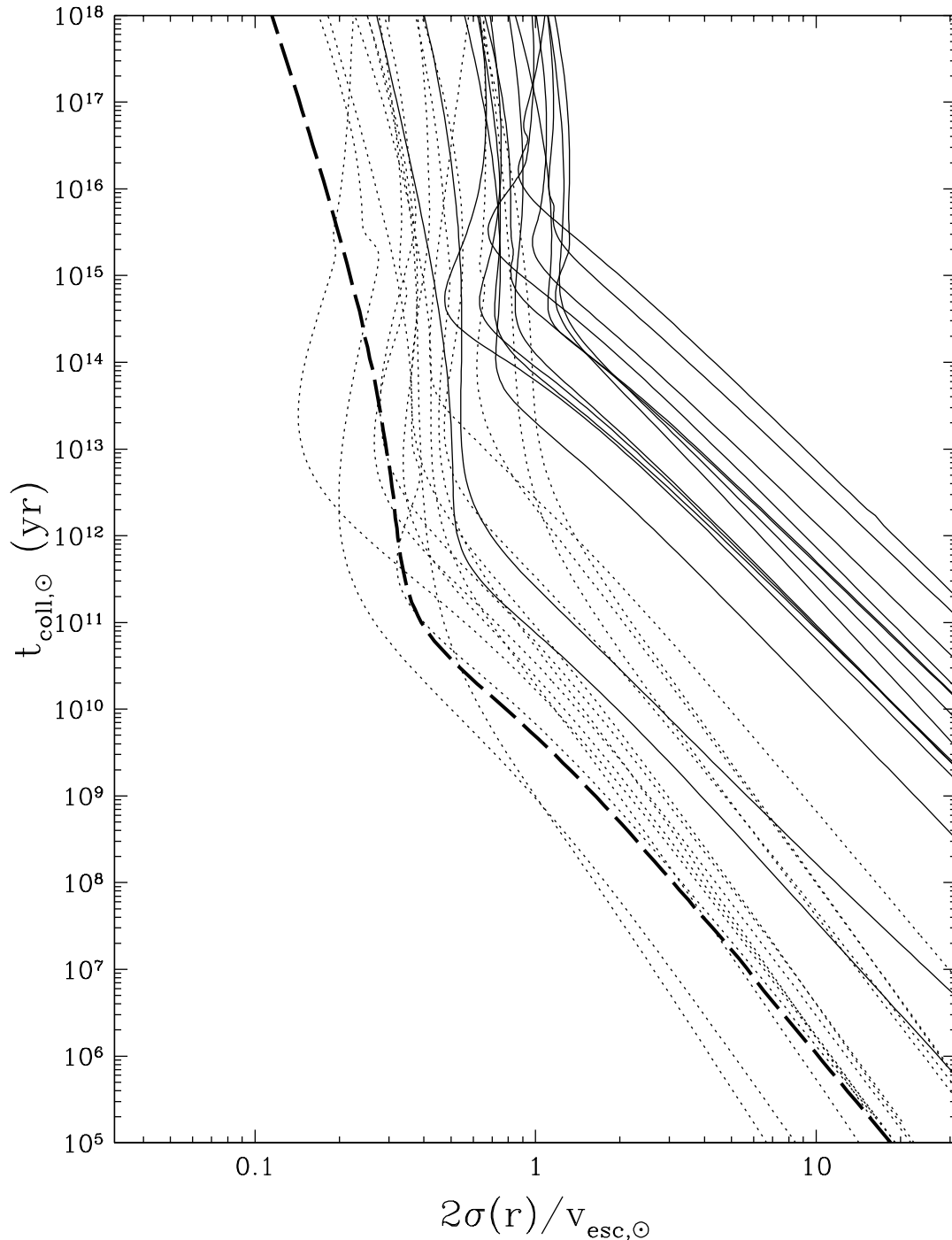


**Figure 2.** Stellar collision timescales  $t_{\text{coll}, \odot}$  as a function of the ratio  $\sigma(r)/v_{\text{esc}, \odot}$ . The quantity  $\sigma(r)$  is the one-dimensional velocity dispersion and  $v_{\text{esc}, \odot} \simeq 620 \text{ km s}^{-1}$  is the escape velocity from stars with solar mass and radius (cf., eq. 1). The galaxies are the same as those in Figure 1. Stars are assumed to all have the solar mass and radius. The line types have the same meaning as those in Figure 1. This figure shows that the velocity dispersion  $\sigma(r)$  is not a monotonic function of radius  $r$ , which is due to the effect of central BHs (note that  $t_{\text{coll}, \odot}$  is a monotonic function of  $r$  in Fig. 1).

Here, the isothermal distributions with the flat and singular stellar densities represent simplified cases for core and power-law galaxies, respectively. As seen from Figure 3(a), most of the solid circles (obtained from actual core galaxies) are located in the region covered by the short dashed lines (those solid circles not covered have break radii  $r_b$  out of the assumed range of  $r_c \sim 10^2\text{--}10^3 \text{ pc}$ ). The mass involved in collisions obtained from the singular isothermal distribution (long dashed line), is basically an upper bound to the masses obtained from actual power-law galaxies (open circles), because the singular stellar density profile is generally steeper than the inner stellar density profiles of most power-law galaxies.

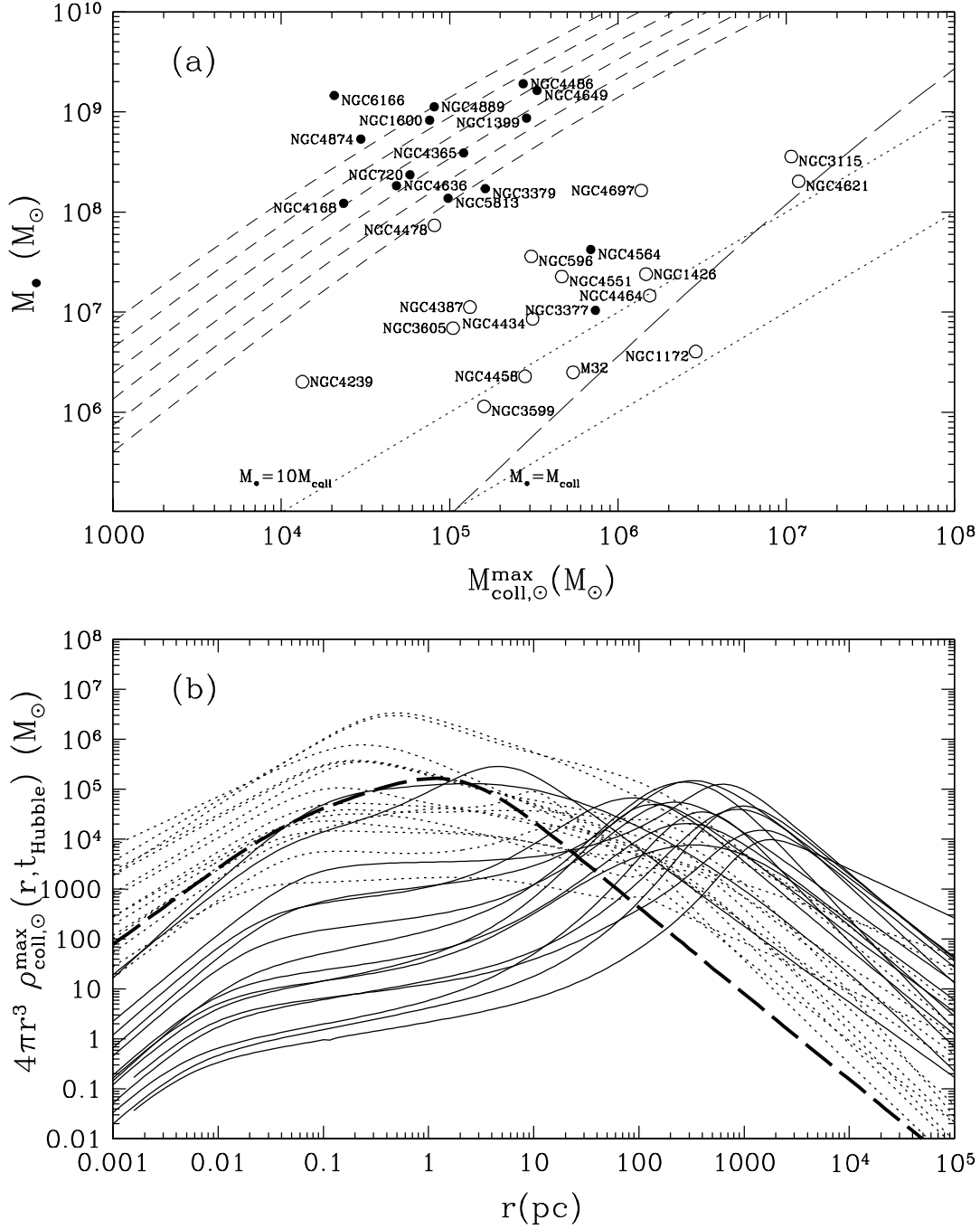


**Figure 3.** Panel (a) shows the total stellar mass involved in collisions  $M_{\text{coll}, \odot}^{\max}(t_{\text{Hubble}})$  (eq. 9) over a Hubble time, versus the central BH mass  $M_{\bullet}$ . The galaxies are the same as those in Figure 1. The BH mass  $M_{\bullet}$  is obtained by the BH mass versus galactic velocity dispersion relation (eq. 20) in Tremaine et al. (2002). Stars are assumed to have the solar mass and radius. The stellar mass involved in collisions is an upper limit to the mass that collisions can contribute to the BH growth (assuming both stars are completely disrupted and the entire gas mass is accreted by the BH). The solid circles represent core galaxies; and the open circles represent power-law galaxies. The dotted lines are the reference lines representing  $M_{\text{coll}, \odot}^{\max}(t_{\text{Hubble}}) = M_{\bullet}$  and  $M_{\text{coll}, \odot}^{\max}(t_{\text{Hubble}}) = 0.1M_{\bullet}$ . The dashed curves give the relation between  $M_{\bullet}$  and  $M_{\text{coll}, \odot}^{\max}(t_{\text{Hubble}})$  in simplified galaxy models with isothermal stellar distributions. The long dashed curve gives the results with singular stellar densities (see eqs. 15–17). The short dashed curves give the results with flat inner stellar densities (eq. 22); reading upwards, the core radius  $r_c$  in equation (22) varies from  $10^2$  pc to  $10^3$  pc with interval  $\Delta \log(r_c/\text{pc}) = 0.2$ . In all cases  $M_{\text{coll}, \odot}^{\max}(t_{\text{Hubble}}) < M_{\bullet}$ . Panel (b) shows  $4\pi r^3 \rho_{\text{coll}, \odot}^{\max}(r, t_{\text{Hubble}})$  as a function of radius  $r$  (cf., eqs. 8 and 9). The peaks of the curves give the location where most of the stellar mass involved in collisions originates. The line types have the same meaning as those in Figure 1. For how the results shown in this Figure change after generalizing to a distribution of masses and radii, see § 3.4.



Figure 3(b) shows  $4\pi r^3 \rho_{\text{coll},\odot}^{\text{max}}(r, t_{\text{Hubble}})$  (cf., eqs. 8 and 9) as a function of galactic radius  $r$ . The peaks or highest parts of these curves represent the regions where most of the stellar mass involved in collisions comes from. The radii where the peaks of the curves are located can be denoted by  $r_{\text{peak}}$ . We have  $\langle v_{\text{rel}}^2 \rangle = 6\sigma^2(r)$  for the typical relative velocity of two colliding stars at radius  $r$ . As seen from Figure 3(b), for core galaxies (solid lines), the peaks of  $4\pi r^3 \rho_{\text{coll},\odot}^{\text{max}}(r)$  are generally located at large radii ( $r_{\text{peak}} \sim 10^2\text{--}10^3$  pc). For power-law galaxies (dotted lines), some of the curves show apparent peaks at small radii ( $r_{\text{peak}} \sim 0.1\text{--}1$  pc); while some have flat-topped profiles covering a large range of radii (e.g.,  $10^{-2}\text{--}10^2$  pc). Note that the mass-to-light ratios of the galaxies are obtained by normalizing to the central velocity dispersion based on spherical and isotropic models fitted to the Nuker-law surface brightness profiles. Thus, given the surface brightness profile and the mass-to-light ratio of the stellar system, we have at  $r \ll r_b$  ( $r_b$ : the break radius, cf., eq. 19)  $n(r) \propto r^{-1}I(r)/m_* \propto r^{-\gamma-1}/m_*$  for power-law galaxies. Now, consider two regions with  $r \ll r_b$  in power-law galaxies:

- In a region with  $t_{\text{coll}}(r) \ll t_{\text{Hubble}}$ , we have

$$r^3 \rho_{\text{coll}}^{\text{max}}(r) \propto r^3 n(r) m_* \propto r^{-\gamma+2}, \quad (23)$$

and since  $\gamma < 2$ ,  $r^3 \rho_{\text{coll}}^{\text{max}}(r)$  increases with increasing galactic radii  $r$  (this applies to the region  $r \lesssim 0.01\text{--}0.1$  pc in Figure 3b).

- In a region with  $t_{\text{coll}}(r) \gg t_{\text{Hubble}}$ , we have (from eqs. 1, 6 and 19)

$$t_{\text{coll}}(r) \propto [n(r)\sigma(r)\Sigma_{ij}]^{-1} \propto \begin{cases} r^{\gamma+1}\sigma(r)^{-1}m_*/a_*^2 & \text{if } \sigma(r) \gg v_{\text{esc}} \\ r^{\gamma+1}\sigma(r)/a_* & \text{if } \sigma(r) \ll v_{\text{esc}}, \end{cases} \quad (24)$$

and

$$r^3 \rho_{\text{coll}}^{\text{max}}(r) \propto r^3 n(r) m_* / t_{\text{coll}}(r) \propto \begin{cases} r^{-2\gamma+1}\sigma(r)a_*^2/m_* & \text{if } \sigma(r) \gg v_{\text{esc}} \\ r^{-2\gamma+1}\sigma(r)^{-1}a_* & \text{if } \sigma(r) \ll v_{\text{esc}}, \end{cases} \quad (25)$$

The (one-dimensional) velocity dispersion  $\sigma(r)$  varies only slowly with the galactic radius  $r$  at  $r > r_H$ , and varies as  $r^{-1/2}$  at  $r < r_H$ , where  $r_H$  is the radius of the sphere of influence of the BH (cf., eq. 21). In the region with  $\sigma(r) \gg v_{\text{esc}}(r)$ , we usually have  $r \ll r_H$ . Thus, according to equation (25), with increasing  $r$ ,  $r^3 \rho_{\text{coll}}^{\text{max}}(r)$  monotonically decreases with radius for power-law galaxies with  $\gamma \gtrsim 0.75$ . For power-law galaxies with  $0.75 \gtrsim \gamma \gtrsim 0.5$ ,  $r^3 \rho_{\text{coll}}^{\text{max}}(r)$  is usually not a monotonic increasing or decreasing function of  $r$  due to the different variation of  $\sigma(r)$  with  $r$  at  $r < r_H$  and  $r > r_H$ .

For power-law galaxies with  $\gamma \gtrsim 0.75$ , since  $r^3 \rho_{\text{coll}}^{\text{max}}(r)$  is an increasing function of  $r$  in the region with  $t_{\text{coll}}(r) \ll t_{\text{Hubble}}$  and is a decreasing function of  $r$  in the region  $r < r_b$  with  $t_{\text{coll}}(r) \gg t_{\text{Hubble}}$ ,  $r^3 \rho_{\text{coll}}^{\text{max}}(r)$  shows a peak in the region with  $t_{\text{coll}}(r) \simeq t_{\text{Hubble}}$ , and the mass involved in collisions comes mainly from small radii  $r_{\text{peak}} \sim 0.1\text{--}1$  pc (cf., Fig. 1a) (see Figure 3b). However, for core galaxies, the peak of  $r^3 \rho_{\text{coll},\odot}^{\text{max}}(r)$  is generally not located around the radii with  $t_{\text{coll}}(r) \simeq t_{\text{Hubble}}$ , but at large radii  $r_{\text{peak}} \sim 10^2\text{--}10^3$  pc where the stellar densities show a break (see the break radii  $r_b$  in eq. 19). In our analysis below, we will focus on power-law galaxies with  $\gamma \gtrsim 0.75$  and core galaxies, which usually can be analytically studied; the results for power-law galaxies with  $0.75 \gtrsim \gamma \gtrsim 0.5$  are usually intermediate cases between the results of those two types of galaxies.

Note that in equation (10), we assume that the stellar density  $n(\mathbf{r})$  is affected only by local stellar collisions. This assumption will not underestimate the mass involved in collisions per unit volume at position  $\mathbf{r}$  if the collision timescale at position  $\mathbf{r}$  is much longer than the age of the stellar system, and this assumption will not affect the estimate of the mass involved in collisions per unit volume at position  $\mathbf{r}$  if stars are on circular orbits. For core galaxies, the mass involved in collisions  $M_{\text{coll}}^{\text{max}}$  comes mainly from near the break radii  $r_b$ , where  $t_{\text{coll}}(r_b, 0) \gg t_{\text{Hubble}}$ ; hence,  $M_{\text{coll}}^{\text{max}} \simeq m_* n(r_b) t_{\text{Hubble}} / t_{\text{coll}}(r_b, 0)$  will not be affected even if we relax the assumption in equation (10). For power-law galaxies with  $\gamma \gtrsim 0.75$ , the mass involved in collisions  $M_{\text{coll}}^{\text{max}}$  comes mainly from the radii  $r_{\text{peak}}$  where  $t_{\text{coll}}(r_{\text{peak}}) \simeq t_{\text{Hubble}}$ , and  $M_{\text{coll}}^{\text{max}}$  is approximately equal to the initial stellar mass within the radius  $r_{\text{peak}}$  (cf., eqs. 13 and 14). Note that the stars on eccentric orbits which are not involved in collisions at their apocenters (e.g.,  $> r_{\text{peak}}$ ), may be involved in collisions at their pericenters (e.g.,  $< r_{\text{peak}}$ ), where the collision timescale is shorter due to high stellar density; and the mass involved in collisions in Figure 3(a) is therefore possibly an underestimate. However, the total stellar mass involved in collisions at radius  $r$  cannot exceed the total mass of stars which may come within radius  $r$ . To find an upper limit to the correction needed for non-locality, we assume that *all* the stars are involved in collisions at their pericenters (if the collision timescale at their pericenter is  $t_{\text{coll}}(r) < t_{\text{Hubble}}$ ) and the total mass involved in collisions per unit volume at position  $\mathbf{r}$  is about  $\min[m_* n(r, 0) t_{\text{Hubble}} / t_{\text{coll}}(r, 0), (1/4\pi r^2) dM_{<r}(r)/dr]$ , where  $M_{<r}(r)$  represents the total mass of stars which may come within radius  $r$  in spherical stellar systems (cf., Fig. 1a in Yu 2002). We find that with these assumptions,  $M_{\text{coll}}^{\text{max}}$  for power-law galaxies with  $\gamma \gtrsim 0.75$  in Figure 3(a) will increase at most by a factor of 2–5 (average 3).

The collision timescale and the stellar mass involved in collisions shown in Figures 1 and 3 are obtained by assuming that all of the stars have the solar mass and radius. Now consider the more general case in which all the stars have identical mass and radius ( $m_*$ ,  $a_*$ ), which are not necessarily the solar values. We find the following changes in the results shown in Figures 1 and 3:

	0.1 M <sub>⊙</sub> , 0.16 R <sub>⊙</sub>		10 M <sub>⊙</sub> , 6.3 R <sub>⊙</sub>	
	core galaxy	power-law galaxy (0.75 ≲ γ ≲ 1.0)	core galaxy	power-law galaxy (0.75 ≲ γ ≲ 1.0)
$r_{\text{peak}}/r_{\text{peak},\odot}$	1	0.2–0.6	1	1.7–4.4
$M_{\text{coll}}^{\text{max}}/M_{\text{coll},\odot}^{\text{max}}$	0.2	0.2–0.6	6	1.7–6.3
$t_{\text{coll}}/t_{\text{coll},\odot}$	4–6		0.2–0.3	

**Table 1.** Changes in the results shown in Figures 1 and 3 (the stellar collision timescale  $t_{\text{coll}}$ , the total stellar mass involved in collisions  $M_{\text{coll}}^{\text{max}}$ , and the radius where most of the stellar mass involved in collisions originates  $r_{\text{peak}}$ ) by assuming that all the stars have mass and radius lower than the solar values (0.1 M<sub>⊙</sub>, 0.16 R<sub>⊙</sub>) or higher than the solar values (10 M<sub>⊙</sub>, 6.3 R<sub>⊙</sub>). See § 3.3.

- The collision timescales vary as  $(m_*/M_\odot)(R_\odot/a_*)^2$  [if  $v_{\text{esc}} \ll \sigma(r)$ ] or  $R_\odot/a_*$  [if  $v_{\text{esc}} \gg \sigma(r)$ ] times  $t_{\text{coll},\odot}(r)$  shown in Figure 1 (cf., eq. 24).
- In the region with  $t_{\text{coll}}(r) \ll t_{\text{Hubble}}$ ,  $4\pi r^3 \rho_{\text{coll}}^{\text{max}}(r)$  is the same as that shown in Figure 3(b) (cf., eq. 23). In the region with  $t_{\text{coll}}(r) \gg t_{\text{Hubble}}$ ,  $4\pi r^3 \rho_{\text{coll}}^{\text{max}}(r)$  varies as  $(a_*/R_\odot)^2 (M_\odot/m_*)$  [if  $v_{\text{esc}} \ll \sigma(r)$ ] or  $a_*/R_\odot$  [if  $v_{\text{esc}} \gg \sigma(r)$ ] times  $4\pi r^3 \rho_{\text{coll},\odot}^{\text{max}}(r)$  shown in Figure 3(b) (cf., eq. 25).
- For core galaxies, the mass involved in collisions  $M_{\text{coll}}^{\text{max}}(t_{\text{Hubble}})$ , which comes mainly from the region near the break radius  $r_b$ , should be  $a_*/R_\odot$  times that shown in Figure 3(a).
- For power-law galaxies with  $\gamma \gtrsim 0.75$ , the mass involved in collisions  $M_{\text{coll}}^{\text{max}}(t_{\text{Hubble}})$  comes mainly from the region  $r \simeq r_{\text{peak}} < r_H$  with  $t_{\text{coll}}(r_{\text{peak}}) \simeq t_{\text{Hubble}}$ ; thus, according to equation (24),  $r_{\text{peak}}$  should be  $[(a_*/R_\odot)^2 (M_\odot/m_*)]^{1/(\gamma+1.5)}$  [if  $\sigma(r) \gg v_{\text{esc}}$ ] or  $(a_*/R_\odot)^{1/(\gamma+0.5)}$  [if  $\sigma(r) \ll v_{\text{esc}}$ ] times that shown in Figure 3(b), and  $M_{\text{coll}}^{\text{max}} [\propto r_{\text{peak}}^3 \rho_{\text{coll}}^{\text{max}}(r_{\text{peak}}) \propto r_{\text{peak}}^3 n(r_{\text{peak}})/t_{\text{Hubble}} \propto r_{\text{peak}}^{-\gamma+2}]$  is about  $[(a_*/R_\odot)^2 (M_\odot/m_*)]^{-(\gamma+2)/(\gamma+1.5)}$  [if  $\sigma(r) \gg v_{\text{esc}}$ ] or  $(a_*/R_\odot)^{-(\gamma+2)/(\gamma+0.5)}$  [if  $\sigma(r) \ll v_{\text{esc}}$ ] times  $M_{\text{coll},\odot}^{\text{max}}$  shown in Figure 3(a).

We now give two examples of the above changes. We first assume that the galaxies are composed of low-mass stars with  $m_* = 0.1 M_\odot$  and  $a_* = 0.16 R_\odot [\simeq (m_*/M_\odot)^\eta, \eta = 0.8, \text{Kippenhahn \& Weigert 1990}]$ . The collision timescales  $t_{\text{coll}}$  will increase by a factor of  $\sim 4$  [ $v_{\text{esc}} \ll \sigma(r)$ ] or  $\sim 6$  [ $v_{\text{esc}} \gg \sigma(r)$ ] compared to those in Figure 1. For core galaxies, the radii where the peaks of  $4\pi r^3 \rho_{\text{coll}}^{\text{max}}(r)$  are located,  $r_{\text{peak}}$ , are generally still around the break radii  $r_b$ , but the stellar mass involved in collisions  $M_{\text{coll}}^{\text{max}}$  will decrease by a factor of  $\sim 0.2$  compared to Figure 3. For power-law galaxies with  $1.0 \gtrsim \gamma \gtrsim 0.75$ ,  $r_{\text{peak}}$  will decrease by a factor of  $\sim 0.2$ – $0.6$ , and so will the stellar masses involved in collisions  $M_{\text{coll}}^{\text{max}}$ . Similarly, we may also obtain the changes by assuming that the galaxies are composed of high-mass stars with  $m_* = 10 M_\odot$  and  $a_* = 6.3 R_\odot$ . The results are summarized in Table 1.

### 3.4 Generalization to a distribution of stellar masses and radii

A realistic stellar system is composed of stars with a distribution of masses and radii, rather than identical stars. To investigate this case, we assume that all stars are formed instantaneously at the formation of the stellar system, and use the following two forms of stellar initial mass function (IMF): one is the Salpeter IMF (Salpeter 1955),

$$\Xi_{\text{Sp}}(m, t = 0) = \begin{cases} A_{\text{Sp}}(m/M_\odot)^{-2.35} & 0.08 \leq m/M_\odot \leq 120, \\ 0 & \text{otherwise;} \end{cases} \quad (26)$$

and the other is the multi-power-law IMF (cf., Kroupa 2002),

$$\Xi_{\text{multi}}(m, t = 0) = A_{\text{multi}} \begin{cases} (m/0.08 M_\odot)^{-0.3} & 0.01 \leq m/M_\odot < 0.08, \\ (m/0.08 M_\odot)^{-1.3} & 0.08 \leq m/M_\odot < 0.5, \\ (0.5 M_\odot/0.08 M_\odot)^{-1.3} (m/0.5 M_\odot)^{-2.3} & 0.5 \leq m/M_\odot < 120.0, \\ 0 & \text{otherwise.} \end{cases} \quad (27)$$

The constants  $A_{\text{Sp}}$  and  $A_{\text{multi}}$  in equations (26) and (27) are determined by  $\int_0^\infty \Xi(m, t = 0) dm = 1$ . The multi-power-law IMF gives a much flatter slope at the low-mass end than the Salpeter IMF. For stars with initial mass  $m$ , the lifetime on the main sequence is about (eq. 9-3 in Binney & Tremaine 1987)

$$t_{\text{MS}} \simeq 10 \text{ Gyr} (m/M_\odot)^{-2.5}. \quad (28)$$

In a stellar system with age  $T_{\text{age}} \sim 10 \text{ Gyr}$ , the mass of stars at the turn-off point  $m_{\text{tf}}$  is about  $1 M_\odot$ . The present mass function of the remaining low-mass main-sequence stars follows their initial mass function  $\Xi(m, 0)$  with  $m \lesssim m_{\text{tf}}$ . These stars are assumed to have radii  $a \simeq (m/M_\odot)^\eta R_\odot$  with  $\eta = 0.8$  (p.208 in Kippenhahn & Weigert 1990). Massive stars ( $\gtrsim 1 M_\odot$ ) usually have lost a significant fraction of their mass and become low-mass remnants (BHs, neutron stars or white dwarfs). We assume that progenitors with mass  $m > 30 M_\odot$  will become BHs with mass  $8 M_\odot$ , progenitors with mass  $30 M_\odot > m > 8 M_\odot$

will become neutron stars with mass  $1.5 M_\odot$  and radius 10 km, and progenitors with mass  $8 M_\odot > m > 1 M_\odot$  will become white dwarfs with mass  $0.6 M_\odot$  and radius  $10^4$  km (e.g., Murphy, Cohn & Durisen 1991). Besides stellar remnants, there also exist other, relatively short lived, post-main-sequence stars (such as red giants, horizontal branch stars or asymptotic giant branch stars etc.) which have evolved from stars with initial mass close to  $m_{\text{tf}}$ .

According to equation (5), we have the collision timescale of main-sequence stars with mass and radius  $(m_i, a_i)$  as follows:

$$t_{\text{coll},i}(r, T_{\text{age}}) \propto \frac{1}{n(r, T_{\text{age}}) \int dm_j da_j \xi(m_j, a_j, T_{\text{age}}) \Sigma_{ij}}. \quad (29)$$

Given the dynamically determined mass-to-light ratio (by normalizing to the central velocity dispersion based on spherical and isotropic models fitted to the surface-brightness profile, see § 3.2) and the observed surface brightness profile, we have the following relation for the stellar number density obtained by using the Eddington formula (eq. 4-140a in Binney & Tremaine 1987)

$$n(r, T_{\text{age}}) \propto \frac{1}{\int_0^\infty dm_j m_j \Xi(m_j, T_{\text{age}})}, \quad (30)$$

which depends on the stellar mass function  $\Xi(m_j, T_{\text{age}})$ . Thus, using equations (1), (29) and (30), we have

$$\begin{aligned} & \frac{t_{\text{coll},i}(r, T_{\text{age}})}{t_{\text{coll},\odot}(r, T_{\text{age}})} \\ & \simeq \int_0^\infty dm_j (m_j / M_\odot) \Xi(m_j, T_{\text{age}}) \\ & \quad \times \begin{cases} 1 / \int_0^{m_{\text{tf}}} dm_j \Xi(m_j, 0) [(a_i + a_j)^2 / (2 R_\odot)^2] & \text{if } \sigma(r) \gg v_{\text{esc},\odot} \\ 1 / \int_0^{m_{\text{tf}}} dm_j \Xi(m_j, 0) [(a_i + a_j) / 2 R_\odot] [(m_i + m_j) / 2 M_\odot] & \text{if } \sigma(r) \ll v_{\text{esc},\odot} \end{cases}, \end{aligned} \quad (31)$$

where  $t_{\text{coll},\odot}$  (see § 3.3 or Fig. 1) is the collision timescale obtained by assuming that all the stars have the solar mass and radius, and  $v_{\text{esc},\odot} = \sqrt{2GM_\odot/R_\odot}$  is the escape velocity from stars with solar mass and radius. The two cases in equation (31) are divided by  $v_{\text{esc},\odot} \sim \sigma(r)$  (cf., eq. 1), because we have  $v_{ij} = \sqrt{2G(m_i + m_j)/(a_i + a_j)} \sim v_{\text{esc},\odot}$  for any collisions of two main-sequence stars with masses  $m_i$  and  $m_j$  in the range  $0.01-1 M_\odot$  [assuming  $a \propto m^\eta$  with  $\eta(=0.8)$  being close to 1] and we assume that the mean relative velocity of two colliding stars is  $\sqrt{\langle v_{\text{rel}} \rangle \langle v_{\text{rel}}^{-1} \rangle^{-1}} \sim \langle v_{\text{rel}}^2 \rangle^{1/2} = \sqrt{6} \sigma(r) \sim \sigma(r)$  (see eq. 1). In equation (29), we have ignored collisions with stellar remnants (BHs, neutron stars or white dwarfs), because the number of stellar remnants (evolved from massive stars) is small compared to that of main-sequence stars (note that mass segregation is ignored) and also the radius of stellar remnants is not large ( $< 1 R_\odot$ ). We have also ignored collisions with other post-main-sequence stars (e.g., red giants) since the number of these stars is also small. Note that the large radius of giants (e.g.,  $\sim 10^2 R_\odot$ ) will increase the collision rates of main-sequence stars, but collisions with red-giant envelopes generally result in little mass loss from either star because the amount of mass contained in the greatly extended envelopes of giants is typically a small fraction of a solar mass and the overlapping area of collisions is quite small relative to the total collision cross section. In addition, as argued by Murphy, Cohn & Durisen (1991), giants undergo significant mass loss in a short amount of time anyway because of stellar winds, and it makes not much difference whether the mass comes from winds or collisions in the sense of providing raw material for the BH growth.

Using equation (29) and assuming that the stellar radius  $a_i = (m_i / M_\odot)^{-0.8} R_\odot$  and the mass of stars at the turn-off point  $m_{\text{tf}} = 1 M_\odot$ , we obtain the collision timescales  $t_{\text{coll},i}$  as a function of stellar mass  $m_i$ . The ratio of collision timescales  $t_{\text{coll},i}/t_{\text{coll},\odot}$  (eq. 31) as a function of stellar mass  $m_i$  is shown in Figure 4 (see  $t_{\text{coll},\odot}$  in Fig. 1). We show the results obtained both by assuming the Salpeter IMF (eq. 26) and by assuming the multi-power-law IMF (eq. 27). As seen from Figure 4, the ratio  $t_{\text{coll},i}/t_{\text{coll},\odot}$  increases from  $\sim 0.6$  to  $\sim 7$  (or to  $\sim 9$ ) with decreasing stellar mass  $m_i$ , from  $m_{\text{tf}}$  to  $0.08 M_\odot$  for the Salpeter IMF (or to  $0.01 M_\odot$  for the multi-power-law IMF), and the difference of the ratios between the two IMFs for  $\sigma(r) \ll v_{\text{esc},\odot}$  and for  $\sigma(r) \gg v_{\text{esc},\odot}$  is less than 30 percent. For the whole population of main-sequence stars, we use equation (6) and the collision timescale  $t_{\text{coll},i}$  shown in Figure 4 to obtain the total collision timescale  $t_{\text{coll}}$ , which is about 3–4 times the timescales  $t_{\text{coll},\odot}$  shown in Figure 1.

According to equation (8), we have the total mass density of main-sequence stars involved in collisions with main-sequence stars with the natural logarithm of their masses in the range  $\ln m_i \rightarrow \ln m_i + d \ln m_i$  per unit time given by:

$$\begin{aligned} \dot{\rho}_{\text{coll},i}^{\text{max}}(r, T_{\text{age}}) d \ln m_i & \propto dm_i \int_0^{m_{\text{tf}}} dm_j (m_i + m_j) \mathcal{R}_{ij}(r, T_{\text{age}}) \\ & \propto dm_i \int_0^{m_{\text{tf}}} dm_j (m_i + m_j) \Xi(m_i, 0) \Xi(m_j, 0) n^2(r, T_{\text{age}}) \Sigma_{ij}; \end{aligned} \quad (32)$$

and using the similar derivation to obtain equation (31), we have the ratio

$$\frac{\dot{\rho}_{\text{coll},i}^{\text{max}}(r, T_{\text{age}})}{2 \dot{\rho}_{\text{coll},\odot}^{\text{max}}(r, T_{\text{age}})} \simeq m_i \Xi(m_i, 0) \left[ \int_0^\infty dm_j (m_j / M_\odot) \Xi(m_j, T_{\text{age}}) \right]^{-2}$$

$$\times \begin{cases} \int_0^{m_{\text{tf}}} dm_j \Xi(m_j, 0) [(a_i + a_j)/(2R_\odot)]^2 [(m_i + m_j)/(2M_\odot)] & \sigma(r) \gg v_{\text{esc}, \odot} \\ \int_0^{m_{\text{tf}}} dm_j \Xi(m_j, 0) [(a_i + a_j)/(2R_\odot)] [(m_i + m_j)/(2M_\odot)]^2 & \sigma(r) \ll v_{\text{esc}, \odot} \end{cases}, \quad (33)$$

where  $\dot{\rho}_{\text{coll}, \odot}^{\text{max}}$  (cf., eq. 8) is the total mass density of main-sequence stars involved in collisions per unit time obtained by assuming that all the stars in the stellar system have solar mass and radius. We put the factor “1/2” in front of  $\dot{\rho}_{\text{coll}, i}^{\text{max}}(r, T_{\text{age}})/\dot{\rho}_{\text{coll}, \odot}^{\text{max}}(r, T_{\text{age}})$  because  $\int_0^{m_{\text{tf}}} \dot{\rho}_{\text{coll}, i}^{\text{max}}(r, T_{\text{age}}) d \ln m_i$  gives twice of the mass involved in collisions (see also the factor “1/2” in eq. 8). We also have the total mass density of main-sequence stars with the natural logarithm of their masses in the range  $\ln m_i \rightarrow \ln m_i + d \ln m_i$  involved in collisions per unit time:

$$\begin{aligned} \dot{\rho}'_{\text{coll}, i}{}^{\text{max}}(r, T_{\text{age}}) d \ln m_i &\propto dm_i \int_0^{m_{\text{tf}}} dm_j m_i \mathcal{R}_{ij}(r, T_{\text{age}}) \\ &\propto dm_i \int_0^{m_{\text{tf}}} dm_j m_i \Xi(m_i, 0) \Xi(m_j, 0) n^2(r, T_{\text{age}}) \Sigma_{ij}, \end{aligned} \quad (34)$$

and

$$\begin{aligned} \frac{\dot{\rho}'_{\text{coll}, i}{}^{\text{max}}(r, T_{\text{age}})}{\dot{\rho}_{\text{coll}, \odot}^{\text{max}}(r, T_{\text{age}})} &\simeq (m_i/M_\odot) m_i \Xi(m_i, 0) \left[ \int_0^\infty dm_j (m_j/M_\odot) \Xi(m_j, T_{\text{age}}) \right]^{-2} \\ &\times \begin{cases} \int_0^{m_{\text{tf}}} dm_j \Xi(m_j, 0) [(a_i + a_j)/(2R_\odot)]^2 & \sigma(r) \gg v_{\text{esc}, \odot} \\ \int_0^{m_{\text{tf}}} dm_j \Xi(m_j, 0) [(a_i + a_j)/(2R_\odot)] [(m_i + m_j)/(2M_\odot)] & \sigma(r) \ll v_{\text{esc}, \odot} \end{cases}. \end{aligned} \quad (35)$$

As in equations (29) and (31), collisions with stellar remnants and other post-main-sequence stars are ignored in equations (32)–(35). We use equations (32)–(35) to obtain  $\dot{\rho}_{\text{coll}, i}^{\text{max}}(r, T_{\text{age}})$  and  $\dot{\rho}'_{\text{coll}, i}{}^{\text{max}}(r, T_{\text{age}})$  as a function of stellar mass  $m_i$ . The ratios of  $\dot{\rho}_{\text{coll}, i}^{\text{max}}/(2\dot{\rho}_{\text{coll}, \odot}^{\text{max}})$  and  $\dot{\rho}'_{\text{coll}, i}{}^{\text{max}}/\dot{\rho}_{\text{coll}, \odot}^{\text{max}}$  as a function of stellar mass  $m_i$  for both the cases  $\sigma(r) \ll v_{\text{esc}, \odot}$  (dotted lines) and  $\sigma(r) \gg v_{\text{esc}, \odot}$  (solid lines) are shown in Figure 5(a) and (b), respectively. We also show the results obtained both by assuming the Salpeter IMF (eq. 26) and by assuming the multi-power-law IMF (eq. 27). In Figure 5(a), the curves of  $\dot{\rho}_{\text{coll}, i}^{\text{max}}/(2\dot{\rho}_{\text{coll}, \odot}^{\text{max}})$  obtained from the Salpeter IMF (with the low-mass end at  $0.08 M_\odot$ ) show a minimum at an intermediate mass between  $0.08$ – $1 M_\odot$  and increase from the minima to both the high-mass end ( $\sim 1 M_\odot$ ) and the low-mass end ( $\sim 0.08 M_\odot$ ), which reflects the fact that the stellar mass involved in collisions comes mainly from collisions between high-mass stars and low-mass stars; and the curves of  $\dot{\rho}'_{\text{coll}, i}{}^{\text{max}}/(2\dot{\rho}_{\text{coll}, \odot}^{\text{max}})$  obtained from the multi-power-law IMF (with the low-mass end at  $0.01 M_\odot$ ) increase with increasing stellar mass  $m_i$ , which reflects the fact that the stellar mass involved in collisions comes mainly from collisions with high-mass stars since the multi-power-law IMF gives a flatter slope at the low-mass end than the Salpeter IMF. Figure 5(b) shows that  $\dot{\rho}'_{\text{coll}, i}{}^{\text{max}}/\dot{\rho}_{\text{coll}, \odot}^{\text{max}}$  obtained from both the Salpeter IMF and the multi-power-law IMF increase with increasing stellar mass  $m_i$ , which reflects that the stellar mass involved in collisions comes mainly from high-mass stars, especially for the multi-power-law IMF since the slope of corresponding curves in Figure 5(b) is steeper. For core galaxies, the total mass of main-sequence stars involved in collisions comes mainly from galactic radii  $r \sim r_b$  [where  $t_{\text{coll}, i}(r) \gg t_{\text{Hubble}}$  and  $\sigma(r) \ll v_{\text{esc}, \odot}$ ], which is found to be  $\sim \int_0^{m_{\text{tf}}} \dot{\rho}_{\text{coll}, i}^{\text{max}} d \ln m_i / (2\dot{\rho}_{\text{coll}, \odot}^{\text{max}}) \simeq 0.4$ – $0.5$  times the result obtained by assuming that the stellar systems have identical stars with solar mass and radius. For power-law galaxies, using equation (18), we find that the total stellar mass involved in collisions  $M_{\text{coll}}$  is smaller than  $M_{\text{coll}, \odot}^{\text{max}}$  (see § 3.3 or Fig. 3) by a factor of  $0.4$ – $0.7$ .

As shown above, after the generalization to a distribution of stellar masses and radii, the total stellar masses involved in collisions decrease compared to those shown in Figure 3(a). In addition, note that not all the collisions result in disruption of stars and not all the gas released by collisions can be accreted onto BHs. Hence, the conclusion obtained from Figure 3 that the mass released by stellar collisions is not enough to account for the central BH growth (especially in bright core galaxies) will not be changed, by more realistic models.

Mass segregation is ignored in the analysis above. This assumption affects little on our result of stellar mass involved in collisions at least for all the core galaxies and most of the power-law galaxies for the following reasons. Our calculation shows that the relaxation timescales of stellar remnants of massive stars (BHs and neutron stars) are higher than the Hubble time for all the core galaxies and are higher than the Hubble time at  $r \gtrsim r_{\text{peak}, \odot}$  for most of the power-law galaxies [only for about four power-law galaxies, the relaxation timescales of the stellar BHs ( $8 M_\odot$ ) are smaller than or approximately equal to the Hubble time at the region  $r \simeq r_{\text{peak}, \odot}$ ].

### 3.5 Material sources for growth of central BHs

As mentioned in § 1, gaseous material for the growth of central BHs in an isolated stellar system may come from stars through three mechanisms (e.g., Murphy, Cohn & Durisen 1991): tidal disruption (or being swallowed whole by central BHs) of stars (mostly on elongated radial orbits), stellar collisions, and stellar evolution. In this subsection, we will compare these three contributors to BH growth.

In a stellar system with a central BH, stars that come within a distance  $r_{\text{tid}} \sim (M_\bullet/m_\star)^{1/3} a_\star$  of the central BH will be tidally disrupted by the BH if  $r_{\text{tid}} \gtrsim r_{\text{Sch}}$  (where  $r_{\text{Sch}} \equiv 2GM_\bullet/c^2$  is the Schwarzschild radius) or swallowed whole by the BH

if  $r_{\text{tid}} \lesssim r_{\text{Sch}}$ . Here, we do not distinguish the above two cases and simply call the total mass of stars which may come within a distance of  $r = \max(r_{\text{tid}}, r_{\text{Sch}})$  as the tidally disrupted mass  $M_{\text{tid}}$ . We use the same method as Magorrian & Tremaine (1999) to obtain  $M_{\text{tid}}$  in realistic galaxies, and the galaxies are assumed to be spherical since flattening or triaxiality of galaxies does not significantly change the results (Magorrian & Tremaine 1999). Figure 6 shows the tidally disrupted stellar mass ( $M_{\text{tid},\odot}$ ) versus the stellar mass involved in collisions ( $M_{\text{coll},\odot}^{\text{max}}$ ) over a Hubble time; in this Figure, the stellar systems are assumed to be composed of identical stars with solar mass and radius. As seen from Figures 3 and 6,  $M_{\text{tid},\odot}$  and  $M_{\text{coll},\odot}^{\text{max}}$  are generally comparable. After the generalization to a distribution of stellar masses and radii (i.e., the Salpeter IMF in eq. 26 or the multi-power-law IMF in eq. 27),  $M_{\text{tid}}$  will increase by a factor of  $\sim 2$ – $3$  (cf., Magorrian & Tremaine 1999), while  $M_{\text{coll}}^{\text{max}}$  will be reduced by a factor of  $\sim 0.4$ – $0.7$ . Considering that not all the collisions result in stellar disruption and not all the gas released by collisions can be accreted onto BHs, tidal disruption is likely to contribute more mass to the central BH growth than stellar collisions. Magorrian & Tremaine (1999) show that tidal disruption contributes significantly to the present BH mass only in faint galaxies  $\lesssim 10^9 L_{\odot}$ . For bright galaxies, our study in this paper shows that neither tidal disruption nor stellar collisions can contribute significantly to their present central BH masses.

Using the simple model of stellar evolution described at the beginning of § 3.4, we may obtain the mass loss caused by stellar evolution if all stars are formed instantaneously at the formation of the stellar system. The mass loss may come either from stellar winds (mainly during giant stages) or from the mass lost by Supernovae II. The total mass loss amounts to about 21 percent of the initial total stellar mass in the initial 1 Gyr and about 7 percent during the interval from 1 Gyr to 10 Gyr for the Salpeter IMF. The corresponding numbers for the multi-power-law IMF are 32% and 10%. (For both of the IMFs, more than forty percent of the mass loss in the initial 1 Gyr comes from stars with initial mass in the range 2.5–8  $M_{\odot}$  or mass lost by stellar winds.) Therefore, mass loss during stellar evolution at the early stage of galaxy evolution is a possible source to feed central BHs if part of the lost mass can lose angular momentum and sink to galactic nuclei.

A final possibility for the material source is that galaxy encounters may concentrate gas in the centers of interacting galaxies to feed BHs (see simulations in Barnes & Hernquist 1996). The gas infall may fuel pre-existing central BHs; or galaxy encounters may trigger a central star burst, which could lead to nuclear activity. For both of the above possibilities, massive BHs form or grow rapidly, early in the universe’s history (e.g., at redshift  $z \sim 2$ – $3$  when galaxy encounters mostly occur in the hierarchical galaxy formation model). This scenario is consistent with one of the arguments made by Yu & Tremaine (2002) that growth of high-mass BHs ( $> 10^8 M_{\odot}$ ) comes mainly from accretion during optically bright QSO phases (which is obtained by studying the relation between the local BH mass function and the QSO luminosity function).

## 4 EFFECTS OF STELLAR COLLISIONS ON COLORS OF GALACTIC CENTERS

As mentioned in § 1, stellar collisions affect the luminosity properties and colors in galactic centers. Stellar collisions may disrupt one or both of the colliding stars to decrease the total luminosity, or the two colliding stars may merge to become a new star with luminosity properties or colors different from its parent stars. In this section, we will first give a general analysis of the effects of stellar collisions on color gradients, and then study these effects in nearby galactic centers, especially two galaxies in the Local Group: M32 and M31.

### 4.1 Color gradients caused by stellar collisions

Color gradients in a galaxy are usually caused by the variation of its stellar population with galactic radius.

If there are no collisions in the stellar system, the surface brightness at color band  $C$  and at projected radius  $R$ , is given by:

$$I_{0,C}(R, T_{\text{age}}) = \int dz \int dmda \xi_0(m, a, T_{\text{age}}) n(r, T_{\text{age}}) L_C(m, a, T_{\text{age}}) \quad (36)$$

$$= J_{0,C}(R, T_{\text{age}}) R f_0(R). \quad (37)$$

Here  $r = \sqrt{R^2 + z^2}$ ,  $\xi_0(m, a, T_{\text{age}})$  is the expected stellar mass and radius function at the present time obtained by assuming an IMF and then only considering the effect of stellar evolution,  $L_C(m, a, T_{\text{age}})$  is the current luminosity emitted by a star with mass and radius  $(m, a)$  at color band  $C$  (in units of the solar  $C$ -band luminosity  $L_{\odot,C}$ ),  $J_{0,C}(r, T_{\text{age}})$  is the luminosity density at galactic radius  $r$  defined by

$$J_{0,C}(r, T_{\text{age}}) \equiv \int dmda \xi_0(m, a, T_{\text{age}}) n(r, T_{\text{age}}) L_C(m, a, T_{\text{age}}) \quad (38)$$

and  $f_0$  is a factor reflecting the projection effect of the surface brightness defined by:

$$f_0(R) \equiv \frac{\int_{-\infty}^{\infty} n(r, T_{\text{age}}) dz}{n(R, T_{\text{age}}) R}. \quad (39)$$

The color index of the surface brightness (at color bands  $C_1$  and  $C_2$ ) at projected radius  $R$  is given by:

$$\mu_{0,C_1}(R) - \mu_{0,C_2}(R) = -2.5 \log[I_{0,C_1}(R)/I_{0,C_2}(R)] + (M_{\odot,C_1} - M_{\odot,C_2}), \quad (40)$$

where  $M_{\odot,C_i}$  is the solar absolute magnitude at color band  $C_i$ . We will call the surface brightness and the color in equations (36) and (40) the ‘‘original’’ surface brightness and color, that is, the brightness and color that would be present in the absence of stellar collisions.

If two stars with masses and radii  $(m_i, a_i)$  and  $(m_j, a_j)$  collide at time  $t'$ , we define  $L_{ij,C}(t, t')$  ( $t \geq t'$ ) as the  $C$ -band luminosity of the collision product at time  $t$ . The luminosity and color of collision products depend on the types of colliding stars, their masses and radii, their relative velocity and impact parameter etc. If both of the two stars are disrupted by the collision, we have  $L_{ij,C}(t, t') = 0$ ; if the two stars merge to be a new star,  $L_{ij,C}(t, t')$  is just the luminosity of the new merged star; and if one or both of the two stars survive the collision,  $L_{ij,C}(t, t')$  represents the total luminosity of the surviving star(s) after the collision. Using the collision rate  $\mathcal{R}_{ij}(r, t')$  in equation (4), the change of the surface brightness at color band  $C$  caused by collisions of two stars with total mass larger than  $m_{ij}$  is given by:

$$\begin{aligned} & I_{\text{coll}, > m_{ij}, C}(R, T_{\text{age}}) \\ &= \frac{1}{2} \int_{\max(m_{ij} - m_{\text{tf}}, 0)}^{m_{\text{tf}}} dm_i \int_{\max(m_{ij} - m_i, 0)}^{m_{\text{tf}}} dm_j \int da_i \int da_j \int dz \int_0^{T_{\text{age}}} dt' \mathcal{R}_{ij}(r, t') \\ & \quad \times [\langle L_{ij,C}(T_{\text{age}}, t', r) \rangle - L_C(m_i, a_i, T_{\text{age}}) - L_C(m_j, a_j, T_{\text{age}})], \end{aligned} \quad (41)$$

where  $\langle L_{ij,C}(T_{\text{age}}, t', r) \rangle$  is the average present luminosity of the collision product of two stars with masses and radii  $(m_i, a_i)$  and  $(m_j, a_j)$  colliding at time  $t'$  and at galactic radius  $r$ . We have the factor ‘‘1/2’’ in front of the integration in equation (41) for the same reason given for equation (8), and we have

$$\frac{1}{2} \int_{\max(m_{ij} - m_{\text{tf}}, 0)}^{m_{\text{tf}}} dm_i \int_{\max(m_{ij} - m_i, 0)}^{m_{\text{tf}}} dm_j = \int_{\max(m_{ij} - m_{\text{tf}}, 0)}^{m_{\text{tf}}} dm_i \int_{\max(m_{ij} - m_i, m_i)}^{m_{\text{tf}}} dm_j. \quad (42)$$

The dependence of the average luminosity  $\langle L_{ij,C}(T_{\text{age}}, t', r) \rangle$  on  $r$  is due to the dependence of the collision outcome on the relative velocity of two colliding stars and the dependence of the relative velocity on  $r$ . In equation (41), we have ignored the radial motion of the collision products, because the radial motion of the collision products is expected to dilute the color gradients caused by collisions; thus, the color gradient obtained from equation (41) is an overestimate. We will mainly analyze the color gradient in the region with  $t_{\text{coll}}(r) \gg T_{\text{age}}$ , where the stellar distribution and population [i.e., the stellar density  $n(r)$  and the stellar mass and radius function  $\xi(m, a)$ ] evolve rather slowly, and we ignore collisions with collision products. Once the initial rapid stellar evolution is complete [massive stars have evolved into stellar remnants and the main-sequence stars have low masses (e.g.,  $\lesssim 1 M_{\odot}$ ) with long lifetime in the main-sequence phase], in the slowly evolved region [where  $t_{\text{coll}}(r) \gg T_{\text{age}}$ ], we have  $\mathcal{R}_{ij}(r, t) \simeq \mathcal{R}_{ij}(r, 0) \simeq \mathcal{R}_{ij}(r, T_{\text{age}})$  in equation (41), i.e.,

$$\begin{aligned} & I_{\text{coll}, > m_{ij}, C}(R, T_{\text{age}}) \\ &= \frac{1}{2} \int_{\max(m_{ij} - m_{\text{tf}}, 0)}^{m_{\text{tf}}} dm_i \int_{\max(m_{ij} - m_i, 0)}^{m_{\text{tf}}} dm_j \int da_i \int da_j \int dz \mathcal{R}_{ij}(r, T_{\text{age}}) \\ & \quad \times \left[ \int_0^{T_{\text{age}}} \langle L_{ij,C}(T_{\text{age}}, t', r) \rangle dt' - L_C(m_i, a_i, T_{\text{age}})T_{\text{age}} - L_C(m_j, a_j, T_{\text{age}})T_{\text{age}} \right]. \end{aligned} \quad (43)$$

Thus, the color index at projected radius  $R$  is given by:

$$\mu_{C_1}(R) - \mu_{C_2}(R) = -2.5 \log \left[ \frac{I_{0,C_1}(R) + I_{\text{coll}, > 0, C_1}(R)}{I_{0,C_2}(R) + I_{\text{coll}, > 0, C_2}(R)} \right] + (M_{\odot,C_1} - M_{\odot,C_2}), \quad (44)$$

and the change of the color index caused by stellar collisions is given by:

$$\Delta\mu_{\text{coll}, C_1 - C_2}(R) = [\mu_{C_1}(R) - \mu_{C_2}(R)] - [\mu_{0,C_1}(R) - \mu_{0,C_2}(R)]. \quad (45)$$

The contribution to the change of the color index from collisions between two stars with total mass  $m_{ij}$  can be seen from the following analysis. According to equations (44) and (45), we have

$$\begin{aligned} & \Delta\mu_{\text{coll}, C_1 - C_2}(R) \\ &= -2.5 \log \left[ 1 + \int d \ln m_{ij} \frac{-dI_{\text{coll}, > m_{ij}, C_1}(R)/d \ln m_{ij}}{I_{0,C_1}(R)} \right] \\ & \quad + 2.5 \log \left[ 1 + \int d \ln m_{ij} \frac{-dI_{\text{coll}, > m_{ij}, C_2}(R)/d \ln m_{ij}}{I_{0,C_2}(R)} \right] \end{aligned} \quad (46)$$

$$\simeq -\frac{2.5}{\ln 10} \int d \ln m_{ij} \left[ \frac{-dI_{\text{coll}, > m_{ij}, C_1}(R)/d \ln m_{ij}}{I_{0,C_1}(R)} - \frac{-dI_{\text{coll}, > m_{ij}, C_2}(R)/d \ln m_{ij}}{I_{0,C_2}(R)} \right] \quad (47)$$

$$\simeq \int d \ln m_{ij} \frac{-dI_{\text{coll},>m_{ij},C_1}(R)/d \ln m_{ij}}{I_{0,C_1}(R)} \Delta\mu_{\text{coll},m_{ij},C_1-C_2}(R), \quad (48)$$

where

$$\begin{aligned} & \frac{dI_{\text{coll},>m_{ij},C_1}(R)}{d \ln m_{ij}} \\ &= -\frac{m_{ij}}{2} \int_{\max(m_{ij}-m_{\text{tf}},0)}^{m_{\text{tf}}} dm_i \int da_i \int da_j \int dz \mathcal{R}_{ij}(r, T_{\text{age}}) \Big|_{m_j=m_{ij}-m_i} \\ & \times \left[ \int_0^{T_{\text{age}}} \langle L_{ij,C}(T_{\text{age}}, t', r) \rangle dt' - L_C(m_i, a_i, T_{\text{age}})T_{\text{age}} - L_C(m_j, a_j, T_{\text{age}})T_{\text{age}} \right], \end{aligned} \quad (49)$$

$$\Delta\mu_{\text{coll},m_{ij},C_1-C_2}(R) = [\mu_{\text{coll},m_{ij},C_1}(R) - \mu_{\text{coll},m_{ij},C_2}(R)] - [\mu_{0,C_1}(R) - \mu_{0,C_2}(R)], \quad (50)$$

$$\mu_{\text{coll},m_{ij},C_1}(R) - \mu_{\text{coll},m_{ij},C_2}(R) = -2.5 \log \left[ \frac{dI_{\text{coll},>m_{ij},C_1}(R)/d \ln m_{ij}}{dI_{\text{coll},>m_{ij},C_2}(R)/d \ln m_{ij}} \right] + (M_{\odot,C_1} - M_{\odot,C_2}). \quad (51)$$

In equations (47) and (48), we use the relation  $\ln(x) = x - 1$  if  $x \rightarrow 1$  where  $\ln x = \Delta\mu_{\text{coll},m_{ij},C_1-C_2}/2.5$ . Equations (47) and (48) are valid for  $I_{\text{coll},>0,C_1}(R)/I_{0,C_1}(R) \ll 1$  and  $I_{\text{coll},>0,C_2}(R)/I_{0,C_2}(R) \ll 1$ ; and for equation (48), we also need  $|\Delta\mu_{\text{coll},m_{ij},C_1-C_2}(R)| \ll 2.5$ . As seen from equation (48), for the collisions of two stars with the natural logarithm of their total mass in the range  $\ln m_{ij} \rightarrow \ln m_{ij} + d \ln m_{ij}$ , whether the change of colors caused by collisions is significant is determined by two factors: (i) the ratio of the change of surface brightness caused by collisions to the original surface brightness,  $d \ln m_{ij}(dI_{\text{coll},>m_{ij},C_1}/d \ln m_{ij})/I_{0,C_1}$ , (ii) the difference between the color index of the change of surface brightness caused by collisions  $\mu_{\text{coll},m_{ij},C_1} - \mu_{\text{coll},m_{ij},C_2}$  and the original color index  $\mu_{0,C_1} - \mu_{0,C_2}$  of the stellar system (i.e.,  $\Delta\mu_{\text{coll},m_{ij},C_1-C_2}$ ).

In this paper, we focus on studying the effects on the color gradient in visible bands caused by collisions between main-sequence stars. We ignore the effects of collisions with post-main-sequence stars because the outcome (especially luminosity and color properties) of these collisions is not well understood and detailed studies of collisions with post-main-sequence stars (e.g., Bailey & Davies 1999) are beyond the scope of this work. We also ignore collisions of compact stellar remnants with main-sequence stars, post-main-sequence stars or even with other compact remnant stars, which usually form “exotic” objects and occur at low rates. We do not intend to study the color gradients in *UV*, far-*UV* or other invisible bands in realistic galaxies, because the luminosities in these bands are more sensitive to post-main-sequence stars (e.g., giants or horizontal branch stars) etc.

#### 4.1.1 Luminosity of collision products of main-sequence stars

The outcome of collisions between main-sequence stars has been investigated by smoothed particle hydrodynamics simulations [e.g., see Sills et al. (1997, 2001) for collisions in globular clusters, and Freitag & Benz (2001) for collisions in galactic centers]. One of the possible outcomes is that the two colliding stars merge to form a new star, which is suggested to be one of the mechanisms to form blue stragglers [for other blue straggler formation mechanisms, see Leonard (1989), Stryker (1993) and Bailyn (1995) etc.]. Here, we simply call the merger products “blue stragglers” (BSs), whether or not they really correspond to the BSs found in observations. The BS is brighter and bluer than its parent stars for two reasons: it may have a larger mass, or the stellar envelope may have a higher helium content if its parent stars have evolved significantly before the collision and the central helium is mixed to the surface of the BS during the collision (e.g., Sills et al. 1997, 2001). The answers to the questions whether collisions of main-sequence stars can form BSs, how much mass is released from stars during stellar coalescence, and how much helium is mixed during the collisions, depend on the masses and radii of the colliding stars, their relative velocity and their impact parameter etc. Hence, these factors also determine what the luminosity properties of BSs formed by stellar collisions will be. Collisions of two stars with low relative velocity (e.g.,  $\lesssim v_{ij}$  in eq. 1) are more likely to lead to stellar coalescence and form BSs; and those with high relative velocity (e.g., at  $r \lesssim 10^{-3}$  pc in galaxies with  $M_{\bullet} \simeq 10^6 M_{\odot}$  or  $r \lesssim 1$  pc in galaxies with  $M_{\bullet} \simeq 10^9 M_{\odot}$  where the velocity dispersion is significantly higher than  $v_{\text{esc},\odot}$ ) are more likely to destroy stars, or the stars may pass through each other and both survive the collision (see Freitag & Benz 2001; Lai, Rasio & Shapiro 1993; Benz & Hills 1987, 1992). Below we will consider several extreme cases of collision products to study the effects of collisions on color gradients. None of the extreme cases are realistic, but they will simplify the complexity of the collision outcome and provide useful limits to the effects caused by stellar collisions.

For the mass of the collision product, we consider two extreme cases: one is that collisions always destroy both of the colliding stars; the other is that collisions always produce BSs and the mass of the BS is the sum of the masses of its parent stars.

We next consider the helium abundance of BSs. A star which has been on the main sequence for time  $\tau$  has created a mass of helium equal to  $\tau\langle L\rangle/(\epsilon c^2)$ , where  $\langle L\rangle$  is the mean luminosity of the star during its main-sequence phase so far, and  $\epsilon = 0.007$  is the efficiency of hydrogen fusion. We define  $Y_0$  and  $Z_0$  as the initial helium abundance and metallicity of the stars.

If a BS is formed by the collision of two main-sequence stars at time  $t$  and the chemical abundance is fully mixed (which is the extreme case of mixing), the resulting helium abundance  $Y_{ij}$  of the BS will be (see eq. 2 in Bailyn & Pinsonneault 1995):

$$Y_{ij} = Y_0 + t_{10} \frac{0.1 M_{\odot}}{m_i + m_j} \frac{\langle L_i \rangle + \langle L_j \rangle}{L_{\odot}} (1 - Y_0), \quad (52)$$

where  $t_{10}$  is the time in units of  $10^{10}$  yr, and  $m_i$  and  $m_j$  are the masses of the two colliding stars. We will consider two extreme cases for the helium abundance of BSs: one is that BSs have the initial helium abundance of their parent stars  $Y_0$ ; and the other is that helium is completely mixed during collisions and BSs have the highest possible helium abundance  $Y_{ij} = 0.1t_{10} + Y_0(1 - 0.1t_{10})$  (eq. 52 for collisions of two main-sequence stars with solar mass).

According to the above treatment, the luminosity of the collision product in equation (41) or (43) is bounded by the following three extreme cases: (i)  $L_{ij,C}(t, t') = 0$ , (ii)

$$L_{ij,C}(t, t') = L_C(m_i + m_j, t - t') \quad (53)$$

with helium abundance  $Y_0$  and metallicity  $Z_0$ , or (iii)  $L_{ij,C}(t, t') = L_C(m_i + m_j, t - t')$  with helium abundance  $Y_{ij} = 0.1t_{10} + Y_0(1 - 0.1t_{10})$  and metallicity  $Z_0$ . Note that the merged BSs are assumed to be equilibrium main-sequence stars after collisions, because the BS should return to the main sequence on the short Kelvin-Helmholtz timescale (e.g.,  $\sim 10^7$  yr for stars with solar mass). In addition, a complete resetting of the nuclear reaction on the main sequence assumed in equation (53) (see the term “ $t - t'$ ”) is unlikely, especially for merged BSs with little helium mixing, which have a shorter main-sequence lifetime (Sills et al. 1997, 2001); and this assumption in equation (53) will give an upper limit to the effect of stellar collisions on color profiles.

## 4.2 Color gradients in M32

In this subsection, we use the dwarf elliptical galaxy M32 in the Local Group as an example to study the color gradients caused by stellar collisions in galactic centers. M32 (NGC 221) is useful for studying stellar collisions because (i) it is the closest elliptical galaxy, (ii) it is compact and its density is high, (iii) it has no visible features of dust or other anomalies (see details in § 4.2.1). M32 has the a shorter stellar collision timescale at *HST* resolution than any other nearby galaxy (see Fig. 1b), and thus we expect that M32 will have the most easily detectable color gradients caused by stellar collisions (if any).

### 4.2.1 Observations

Both photometry (in the optical/infrared bands) and spectroscopy suggest that the center of M32 has a relatively homogeneous stellar population without strong gradients in age or metallicity. No evidence of features such as an inner disk, dust, or any other structure is visible in the *HST* WFPC2 optical images and the Near Infrared Camera and Multi-Object Spectrometer (NICMOS) images (Lauer et al. 1998; Corbin, O’Neil & Rieke 2001). A Nuker-law fit (eq. 19) to the *V*-band surface brightness profile at  $r < 1''$  gives  $\alpha = 1.39 \pm 0.82$ ,  $\beta = 1.47 \pm 0.16$ ,  $\gamma = 0.46 \pm 0.14$ ,  $I_b$  corresponding to  $\mu_b = 12.91 \pm 0.31$ , and  $r_b = 0.47'' \pm 0.15''$  (Lauer et al. 1998). The central cusp of the surface brightness profile of M32 continues to rise into the *HST* resolution limit; thus there is only a lower limit on the central density  $\rho_0 > 10^7 M_{\odot} \text{pc}^{-3}$  (Lauer et al. 1998). The BH mass of M32 is about  $(2.5 \pm 0.5) \times 10^6 M_{\odot}$  and the stellar *I*-band mass-to-light ratio (determined from dynamical models) is  $M/L_I = (1.85 \pm 0.15) M_{\odot}/L_{\odot,I}$  (Verolme et al. 2002). The fit to the M32 color profiles for  $0.1'' < r < 10''$  gives an essentially flat color index as a function of projected radius  $R$  (Lauer et al. 1998):

$$\mu_{\text{obs},V} - \mu_{\text{obs},I} = (1.237 \pm 0.002) - (0.009 \pm 0.005) \log(R/1''). \quad (54)$$

and

$$\mu_{\text{obs},U} - \mu_{\text{obs},V} = (1.216 \pm 0.004) - (0.023 \pm 0.008) \log(R/1''), \quad (55)$$

where  $\mu_{\text{obs}}$  is the observational surface brightness in mag arcsec $^{-2}$ . The absorption line indexes in the optical bands also show no radial gradients from  $1''$  to  $\sim 10''$  (del Burgo et al. 2001). *HST* NICMOS imaging of the core of M32 shows that the near-infrared surface brightness profiles can be fitted by the same form as that fitted to the optical images (Corbin, O’Neil & Rieke 2001) and no strong gradients are found in the infrared color profiles (Peletier 1993; Corbin, O’Neil & Rieke 2001). The spatial distribution of the brightest stars in the infrared also follows the optical light profile outside  $2''$  of the nucleus of M32 (Davidge et al. 2000). The absence of gradients in both colors and absorption line indexes indicates that the stars are coeval or that the stars have been mixed considerably in the inner region of M32. By fitting the mean values of the spectral indexes and colors for the inner regions of M32 to the stellar population synthesis model in Vazdekis et al. (1996), del Burgo et al. (2001) find that the population in the core of M32 can be modeled as a single stellar population of an intermediate age ( $\simeq 4$  Gyr) and solar abundance. Note that the IMFs used in the model of Vazdekis et al. (1996) are not exactly the same as equations (26) and (27) (e.g., they have different lower and upper limits of the stellar mass range etc.). In this paper, we will



focus on the results obtained by using the Salpeter IMFs in equation (26), but our conclusions will not be significantly affected if we use the IMFs in Vazdekis et al. (1996) or equation (27). We will study whether collisions between main-sequence stars can produce a color gradient in M32 in visible bands.

#### 4.2.2 Expected color gradients caused by collisions between main-sequence stars

Assume that the center of M32 is composed of a single stellar population of an intermediate age ( $\simeq 4$  Gyr) with a Salpeter IMF (eq. 26) and solar abundance (see § 4.2.1), and that the stellar population evolves as described in § 3.4. In such a system, the turn-off stars have a mass  $m_{\text{tf}} \simeq 1.3 M_{\odot}$  (set  $t_{\text{MS}} = 4$  Gyr in eq. 28).

In § 4.1.1, we have described three extreme cases of the luminosity of collision products  $L_{ij,C}(t', t)$ . Using equations (36), (40)–(45), and the luminosity of main-sequence stars  $L_C(m, t)$  obtained from the Padova stellar evolutionary tracks (Girardi et al. 2000), we do the numerical calculation for cases (i) and (ii) and find that stellar collisions cannot cause observable color gradients in color indexes  $\mu_U - \mu_V$  and  $\mu_V - \mu_I$  in the center of M32 (i.e.,  $\Delta\mu_{\text{coll},U-V} < 0.02$  mag and  $\Delta\mu_{\text{coll},V-I} < 0.02$  mag at  $R > 0.1''$ , see Fig. 10 below). In case (iii), the evolutionary tracks of stars with the required chemical abundance is not provided in Girardi et al. (2000) or any other published literature that we are aware of. However, we shall argue that the difference in the chemical abundance in case (iii) will not significantly affect our conclusions obtained in cases (ii).

The above numerical results (i.e., no observable color gradients are expected to be caused by collisions between main-sequence stars in M32) may be understood in the following semi-analytic way. We consider the case in which stellar collisions always lead to stellar coalescence, i.e., case (ii). Using equation (53), we have  $\int_0^{T_{\text{age}}} L_{ij,C}(T_{\text{age}}, t') dt' = \int_0^{T_{\text{age}}} L_C(m_i + m_j, T_{\text{age}} - t') dt' = \int_0^{T_{\text{age}}} L_C(m_i + m_j, t) dt$ , and the surface brightness contributed by the BSs which are formed by collisions of two stars with total mass higher than  $m_{ij}$  is given by (cf., eq. 43):

$$I_{\text{coll},>m_{ij},C}^{\text{BS}}(R, T_{\text{age}}) = \frac{1}{2} \int_{\max(m_{ij}-m_{\text{tf}},0)}^{m_{\text{tf}}} dm_i \int_{\max(m_{ij}-m_i,0)}^{m_{\text{tf}}} dm_j \int da_i \int da_j \int_{-\infty}^{\infty} dz \mathcal{R}_{ij}(r, T_{\text{age}}) \times \int_0^{T_{\text{age}}} L_C(m_i + m_j, t) dt \quad (56)$$

$$= J_{\text{coll},>m_{ij},C}^{\text{BS}}(R, T_{\text{age}}) f_{\text{coll}}(R) \quad (57)$$

where  $J_{\text{coll},>m_{ij},C}^{\text{BS}}(r, T_{\text{age}})$  is the luminosity density contributed by the BSs which are formed by collisions of two stars with total mass higher than  $m_{ij}$  at galactic radius  $r$ :

$$J_{\text{coll},>m_{ij},C}^{\text{BS}}(r, T_{\text{age}}) \equiv \frac{1}{2} \int_{\max(m_{ij}-m_{\text{tf}},0)}^{m_{\text{tf}}} dm_i \int_{\max(m_{ij}-m_i,0)}^{m_{\text{tf}}} dm_j \int da_i \int da_j \mathcal{R}_{ij}(r, T_{\text{age}}) \times \int_0^{T_{\text{age}}} L_C(m_i + m_j, t') dt'. \quad (58)$$

Here  $f_{\text{coll}}(R)$  is a factor reflecting the projection effect of the surface brightness. According to equations (1)–(4) and (56)–(58), we approximately have

$$f_{\text{coll}}(R) \simeq \frac{\int_{-\infty}^{\infty} n^2(r, T_{\text{age}}) \sigma(r) [1 + v_{\text{esc},\odot}^2/6\sigma^2(r)] dz}{n^2(R, T_{\text{age}}) \sigma(R) [1 + v_{\text{esc},\odot}^2/6\sigma^2(R)] R}, \quad (59)$$

where  $v_{ij} \simeq v_{\text{esc},\odot}$ ,  $\langle v_{\text{rel}} \rangle \propto \sigma(r)$  and  $\langle v_{\text{rel}} \rangle \langle v_{\text{rel}}^{-1} \rangle^{-1} \simeq \langle v_{\text{rel}}^2 \rangle = 6\sigma^2(r)$  [ $f_{\text{coll}}(R)$  is not sensitive to the factor “6” in front of  $\sigma^2(r)$ ] are assumed (see eq. 1). Thus, as in the derivation in equations (44)–(51), we may obtain the change of the color index caused by BSs given by:

$$\Delta\mu_{\text{coll},C_1-C_2}^{\text{BS}}(R) \simeq \frac{f_{\text{coll}}(R)}{f_0(R)} \int d \ln m_{ij} \frac{-dJ_{\text{coll},>m_{ij},C_1}^{\text{BS}}(R)/d \ln m_{ij}}{J_{0,C_1}(R)} \Delta\mu_{\text{coll},m_{ij},C_1-C_2}^{\text{BS}}(R) \quad (60)$$

where

$$\frac{dJ_{\text{coll},>m_{ij},C_1}^{\text{BS}}}{d \ln m_{ij}} = -\frac{m_{ij}}{2} \int_{\max(m_{ij}-m_{\text{tf}},0)}^{m_{\text{tf}}} dm_i \int da_i \int da_j \mathcal{R}_{ij}(r, T_{\text{age}}) \Big|_{m_j=m_{ij}-m_i} \times \int_0^{T_{\text{age}}} L_C(m_{ij}, t) dt, \quad (61)$$

$$\Delta\mu_{\text{coll},m_{ij},C_1-C_2}^{\text{BS}}(R) = [\mu_{\text{coll},m_{ij},C_1}^{\text{BS}}(R) - \mu_{\text{coll},m_{ij},C_2}^{\text{BS}}(R)] - [\mu_{0,C_1}(R) - \mu_{0,C_2}(R)], \quad (62)$$

$$\begin{aligned}
& \mu_{\text{coll},m_{ij},C_1}^{\text{BS}}(R) - \mu_{\text{coll},m_{ij},C_2}^{\text{BS}}(R) \\
&= -2.5 \log \left[ \frac{dJ_{\text{coll},>m_{ij},C_1}^{\text{BS}}(R)/d \ln m_{ij}}{dJ_{\text{coll},>m_{ij},C_2}^{\text{BS}}(R)/d \ln m_{ij}} \right] + (M_{\odot,C_1} - M_{\odot,C_2}) \\
&= -2.5 \log \left[ \frac{\int_0^{T_{\text{age}}} L_{C_1}(m_{ij}, t) dt}{\int_0^{T_{\text{age}}} L_{C_2}(m_{ij}, t) dt} \right] + (M_{\odot,C_1} - M_{\odot,C_2}). \tag{63}
\end{aligned}$$

Equation (60) is valid for  $[f_{\text{coll}}(R)J_{\text{coll},>0,C_1}^{\text{BS}}(R)]/[f_0(R)J_{0,C_1}(R)] \ll 1$ ,  $[f_{\text{coll}}(R)J_{\text{coll},>0,C_2}^{\text{BS}}(R)]/[f_0(R)J_{0,C_2}(R)] \ll 1$  and  $|\Delta\mu_{\text{coll},m_{ij},C_1-C_2}^{\text{BS}}(R)| \ll 2.5$ . Equation (60) shows that for the collisions of two stars with total mass in the range  $\ln m_{ij} \rightarrow \ln m_{ij} + d \ln m_{ij}$ , whether the effect of BSs on the color gradient is significant at projected radius  $R$  is controlled by three factors: (i) the ratio of the luminosity density  $d \ln m_{ij} (dJ_{\text{coll},>m_{ij},C_1}^{\text{BS}}/d \ln m_{ij})/J_{0,C_1}$  at galactic radius  $r = R$ ; (ii) the difference between the color of BSs and the original color of galactic centers,  $\Delta\mu_{\text{coll},m_{ij},C_1-C_2}^{\text{BS}}$ ; and (iii) the projection effect  $f_{\text{coll}}/f_0$  (see eqs. 39 and 59).

Below, we will give a quantitative estimate to the three factors in equation (60). If the center of M32 is composed of identical stars with solar mass and radius, we may use the surface brightness profile of M32 and its mass-to-light ratio  $\Upsilon$  determined from dynamical models to get its stellar mass density or stellar number density  $n_{\odot}(r)$ . In such a system, we define the luminosity density contributed by BSs formed by collisions between solar-type stars as  $J_{\text{coll},\odot,C}^{\text{BS}}(r)$ ; and according to equation (43), we have

$$\begin{aligned}
\frac{J_{\text{coll},\odot,C}^{\text{BS}}(r)}{J_{0,C}(r)} &\simeq \frac{[n_{\odot}(r)/2t_{\text{coll},\odot}(r)] \int_0^{T_{\text{age}}} L_C(2M_{\odot}) dt}{n_{\odot}(r)L_C(M_{\odot})/\Upsilon_C} \simeq \frac{\Upsilon_C t_{\text{MS}}(1M_{\odot})}{t_{\text{coll},\odot}(r)} \\
&\simeq 0.2 \frac{10^{11} \text{ yr}}{t_{\text{coll},\odot}(r = 0.1'')} \frac{t_{\text{coll},\odot}(r = 0.1'')}{t_{\text{coll},\odot}(r)} \frac{\Upsilon_C}{2}, \tag{64}
\end{aligned}$$

where  $\int_0^{T_{\text{age}}} L_C(2M_{\odot}) dt \simeq L_C(1M_{\odot})t_{\text{MS}}(1M_{\odot})$  is assumed (i.e. the time-integrated luminosity of main-sequence stars is assumed to have  $\int_0^{T_{\text{age}}} L_C(m, t) dt \propto m$  for  $m \geq m_{\text{tf}}$ ), and  $t_{\text{MS}}(1M_{\odot}) = 10^{10}$  yr. If the stars have a distribution of masses and radii, according to equation (58), we have the ratio of the luminosity density contributed by BSs as follows (similarly as eqs. 31, 33 and 35):

$$\begin{aligned}
& \frac{J_{\text{coll},>m_{ij},C}^{\text{BS}}(r)}{J_{\text{coll},\odot,C}^{\text{BS}}(r)} \\
&\simeq \left[ \int_0^{\infty} dm_i (m_i/M_{\odot}) \Xi(m_i, T_{\text{age}}) \right]^{-2} \\
&\times \int_{\max(m_{ij}-m_{\text{tf}}, 0)}^{m_{\text{tf}}} dm_i \int_{\max(m_{ij}-m_i, 0)}^{m_{\text{tf}}} dm_j \Xi(m_i, 0) \Xi(m_j, 0) \frac{\int_0^{T_{\text{age}}} L_C(m_i + m_j, t) dt}{\int_0^{T_{\text{age}}} L_C(2M_{\odot}, t) dt} \\
&\times \begin{cases} [(a_i + a_j)/(2R_{\odot})]^2 & \text{if } \sigma(r) \gg v_{\text{esc},\odot} \\ [(a_i + a_j)/(2R_{\odot})][(m_i + m_j)/(2M_{\odot})] & \text{if } \sigma(r) \ll v_{\text{esc},\odot} \end{cases}. \tag{65}
\end{aligned}$$

We assume the following relation for the luminosity of main-sequence stars:

$$\int_0^{T_{\text{age}}} L_C(m, t) dt \propto \begin{cases} m & \text{if } m \geq m_{\text{tf}} \\ m^{\eta_L} & \text{if } m < m_{\text{tf}} \end{cases}. \tag{66}$$

(i.e., the luminosity of main-sequence stars is assumed to be  $L_C(m, t) \propto m^{\eta_L}$ ;  $\eta_L = 3.5$ ). Using equations (65) and (66), we show in Figure 7 the ratio of the luminosity density  $J_{\text{coll},>m_{ij},C}^{\text{BS}}/J_{\text{coll},\odot,C}^{\text{BS}}$  (solid lines) and its derivative  $|dJ_{\text{coll},>m_{ij},C}^{\text{BS}}/d \ln m_{ij}|/J_{\text{coll},\odot,C}^{\text{BS}}$  (dotted lines) as a function of stellar mass  $m_{ij}$ . We show the results for both of the two cases  $\sigma(r) \gg v_{\text{esc},\odot}$  and  $\sigma(r) \ll v_{\text{esc},\odot}$  in equation (65), and we have

$$\frac{J_{\text{coll},>0,C}^{\text{BS}}(r)}{J_{\text{coll},\odot,C}^{\text{BS}}(r)} \simeq 0.3. \tag{67}$$

The peak of the derivative  $|dJ_{\text{coll},>m_{ij},C}^{\text{BS}}/d \ln m_{ij}|/J_{\text{coll},\odot,C}^{\text{BS}}$  is located at  $m_{ij} \simeq m_{\text{tf}}$ , which represents that most of the luminosity contributed by BSs comes from collisions between two main-sequence stars with total mass  $m_{ij} \simeq m_{\text{tf}}$ .

To obtain the difference between the color of BSs and the original colors of the center in M32 in the absence of stellar collisions (i.e.,  $\Delta\mu_{\text{coll},m_{ij},C_1-C_2}^{\text{BS}}$  in eq. 62), we use the Padova stellar evolutionary track (Girardi et al. 2000) to obtain the color indexes of time-integrated luminosity  $\int_0^{T_{\text{age}}} L_C(m_{ij}, t) dt$  of stars during their main-sequence phases as a function of

stellar mass  $m_{ij}$ ,  $\Lambda_{C_1}(m_{ij}) - \Lambda_{C_2}(m_{ij})$ , defined by (cf., eq. 63):

$$\Lambda_{C_1}(m_{ij}) - \Lambda_{C_2}(m_{ij}) \equiv -2.5 \log \left[ \frac{\int_0^{T_{\text{age}}} L_{C_1}(m_{ij}, t) dt}{\int_0^{T_{\text{age}}} L_{C_2}(m_{ij}, t) dt} \right] + (M_{\odot, C_1} - M_{\odot, C_2}) \quad (68)$$

(in the integration  $\int_0^{T_{\text{age}}} L_C(m_{ij}, t) dt$ , even if we include the luminosity during the post-main-sequence phase, our conclusion will not be affected). Combining equations (63) and (68), we have

$$\mu_{\text{coll}, m_{ij}, C_1}^{\text{BS}} - \mu_{\text{coll}, m_{ij}, C_2}^{\text{BS}} = \Lambda_{C_1}(m_{ij}) - \Lambda_{C_2}(m_{ij}). \quad (69)$$

The  $\Lambda_U(m_{ij}) - \Lambda_V(m_{ij})$  and  $\Lambda_V(m_{ij}) - \Lambda_I(m_{ij})$  for stars with solar abundance are shown as a function of stellar mass  $m_{ij}$  in Figure 8. The horizontal lines in Figure 8 give the observed color indexes of  $\mu_{\text{obs}, U} - \mu_{\text{obs}, V}$  (thin solid line) and  $\mu_{\text{obs}, V} - \mu_{\text{obs}, I}$  (thin dashed line) in the center of M32 at  $R = 1''$  (eqs. 54 and 55). As seen from Figure 8, for color index  $\Lambda_U(m_{ij}) - \Lambda_V(m_{ij})$  (thick solid line), the stars with mass  $m_{ij} \gtrsim 0.9 M_{\odot}$  are bluer than the center of M32; and for color index  $\Lambda_V(m_{ij}) - \Lambda_I(m_{ij})$  (thick dashed line), the stars with mass  $m_{ij} \gtrsim 0.7 M_{\odot}$  are bluer than the galactic center of M32. In Figure 8, at  $m_{ij} \simeq m_{\text{tf}}$ , where the peak of  $|dI_{\text{coll}, > m_{ij}, C}^{\text{BS}}/d \ln m_{ij}|/I_{\text{coll}, \odot, C}$  is located, we have

$$\Delta \mu_{\text{coll}, m_{ij}, U-V}^{\text{BS}} = [\Lambda_U(m_{ij}) - \Lambda_V(m_{ij})] - [\mu_{\text{obs}, U} - \mu_{\text{obs}, V}] \simeq -0.7 \quad (70)$$

and

$$\Delta \mu_{\text{coll}, m_{ij}, V-I}^{\text{BS}} = [\Lambda_V(m_{ij}) - \Lambda_I(m_{ij})] - [\mu_{\text{obs}, V} - \mu_{\text{obs}, I}] \simeq -0.6. \quad (71)$$

Using equations (39) and (59), we obtain the projection factors  $f_0(R)$  and  $f_{\text{coll}}(R)$  of M32 and their ratio  $f_{\text{coll}}(R)/f_0(R)$  as a function of projected radius  $R$ , which are shown in Figure 9. The results in the region not resolved by the *HST* ( $2R < 0.1''$ ) are obtained by extrapolating the Nuker-law fitted surface brightness profile inwards. Figure 9 shows that  $f_{\text{coll}}(R = 0.1'')/f_0(R = 0.1'')$  weakly depends on  $R$  and

$$\frac{f_{\text{coll}}(R = 0.1'')}{f_0(R = 0.1'')} \simeq 0.5. \quad (72)$$

Using equation (60), we have the following relation for the change of the color index caused by stellar collisions:

$$|\Delta \mu_{\text{coll}, C_1-C_2}^{\text{BS}}(R)| < \frac{f_{\text{coll}}(R)}{f_0(R)} \frac{J_{\text{coll}, > 0, C_1}^{\text{BS}}(R)}{J_{0, C_1}(R)} |\Delta \mu_{\text{coll}, m_{\text{tf}}, C_1-C_2}^{\text{BS}}|, \quad (73)$$

where we use the value of  $\Delta \mu_{\text{coll}, m_{ij}, C_1-C_2}^{\text{BS}}$ , at  $m_{ij} \simeq m_{\text{tf}}$  since the peak of  $|dI_{\text{coll}, > m_{ij}}^{\text{BS}}/d \ln m_{ij}|/I_0$  is located at  $m_{ij} \simeq m_{\text{tf}}$  (note that  $|dI_{\text{coll}, > m_{ij}}^{\text{BS}}/d \ln m_{ij}|/I_0$  decrease sharply from  $m_{ij} \simeq m_{\text{tf}}$  to both high-mass and low-mass ends in Figure 7 and  $\Lambda_{C_1}(m_{ij}) - \Lambda_{C_2}(m_{ij})$  change mildly in the whole mass range in Figure 8). Using equations (64), (67), and (70)–(72) in equation (73), we have

$$0 > \left\{ \frac{\Delta \mu_{\text{coll}, V-I}^{\text{BS}}(R)}{\Delta \mu_{\text{coll}, U-V}^{\text{BS}}(R)} \right\} > -0.03 \text{ mag} \left[ \frac{t_{\text{coll}, \odot}(R)}{t_{\text{coll}, \odot}(R = 0.1'')} \right], \quad (74)$$

where the collision timescale  $t_{\text{coll}, \odot}(R = 0.1'') \simeq 10^{11}$  yr (see Fig. 1) for M32 is used. Inequality (74) gives an upper limit of the blueing caused by collisions between main-sequence stars, which shows that it is almost impossible for stellar collisions to cause observable blueing at  $R \gtrsim 0.1''$  in the center of M32. But inequality (74) does not exclude the possibility that stellar collisions can cause a color difference  $> 0.02$  mag in the much inner region at  $R < 0.1''$ . Note that inequality (74) is invalid in the region [e.g.,  $R \lesssim 0.01''$  with  $t_{\text{coll}}(R) \lesssim T_{\text{age}}$ ] where the approximation in equations (48) and (60) is invalid.

In the assumed extreme case (iii) on the luminosity of collision products, BSs have a different Helium abundance from case (ii). But the difference in Helium abundance will not significantly affect the luminosity and colors of BSs or the terms  $J_{\text{coll}, > m_{ij}, C}^{\text{BS}}(R)/J_{0, C}(R)$  and  $\Delta \mu_{\text{coll}, m_{ij}, C_1-C_2}^{\text{BS}}(R)$  (cf., eq. 60), and hence will not affect our conclusions for the following reasons. In cases (ii) and (iii), the mean molecular weights  $\mu_w = (2X + 0.75Y + 0.5Z)^{-1}$  are about 0.62 and 0.63 (Helium abundance  $Y = 0.28$  and  $0.31$ ), respectively. For main-sequence stars with same mass, the increase in the mean molecular weights can only increase the luminosity by about eight percent ( $L \propto \mu_w^4$ , see eq. 20.20 in Kippenhahn & Weigert 1990). The radius of the stars ( $a_* \propto \mu_w^{0.6}$ , see eq. 20.21 in Kippenhahn & Weigert 1990) depends weakly on the mean molecular weight. Thus, the increase in the mean molecular weight and stellar radius will cause the increase of the effective temperature of the star ( $T_{\text{eff}} \propto L/R^2 \propto \mu_w^{2.8}$ ) by about five percent, which may make main-sequence stars with mass around  $m_{\text{tf}}$  (with effective temperatures  $T_{\text{eff}} \sim 6 \times 10^3$  K) bluer only by less than 0.1 mag in  $\Lambda_U - \Lambda_V$  and  $\Lambda_V - \Lambda_I$  (or  $\Delta \mu_{\text{coll}, m_{\text{tf}}, U-V}^{\text{BS}}$  and  $\Delta \mu_{\text{coll}, m_{\text{tf}}, V-I}^{\text{BS}}$ ). Therefore, the results obtained for case (iii) (considering the change of the luminosity and colors of BSs caused by helium mixing) should not be significantly different from those obtained for case (ii).

Inequality (74) only provides the effect on color indexes caused by BSs. Including the effect of removing the luminosity of parent stars from the galactic center [i.e., “the term  $-L_C(m_i, a_i, T_{\text{age}}) - L_C(m_j, a_j, T_{\text{age}})$ ” in eq. 41] will not make the galactic center become bluer because the decrease of the luminosity caused by destruction of main-sequence stars comes mainly from

destruction of high-mass stars (just as most of the mass density involved in collisions come from destruction of high-mass stars shown in Fig. 7), which are usually bluer than the center of M32 (cf., Fig. 8). If collisions of main-sequence stars are assumed to always lead to destruction of main-sequence stars and no BSs are formed [i.e. case (i)], using the above similar analysis for the effects by BSs, we find that there will be no observable reddening at  $R > 0.1''$  of M32, either.

Figure 10 shows our numerical results for the color indexes  $\mu_V(R) - \mu_I(R)$  and  $\mu_U(R) - \mu_V(R)$  in M32, obtained by using equations (36), (40)–(45) and considering the luminosity of collision products in case (i) and case (ii) (dashed line and solid line) as described in § 4.1.1. We use the observed color indexes (eqs. 54 and 55) as the original color index  $\mu_{0,C_1} - \mu_{0,C_2}$ . Figure 10 shows that collisions of main-sequence stars cannot cause observable color changes in the visible bands at  $R > 0.1''$  in M32, which is consistent with the observation that no color gradients are seen in M32 by *HST*; and at even smaller radii, stellar collisions are likely to cause the color difference larger than  $> 0.02$  mag (e.g., at most 0.08 mag at  $R = 0.02''$ ). The above analysis and numerical results are only valid if  $t_{\text{coll}}(R) \gtrsim T_{\text{age}}$ . In the region with  $t_{\text{coll}}(R) \lesssim T_{\text{age}}$  (e.g.,  $R \lesssim 0.01''$ ), it is possible that most of the main-sequence stars have experienced collisions. If we extrapolate the observed *V*-band surface brightness profile inward and assume that the surface brightness in the region with  $t_{\text{coll},\odot}(R) \lesssim T_{\text{age}}$  has the color of BSs described in equations (70) and (71), and then use the above numerical results of the surface brightness in the region with  $t_{\text{coll},\odot}(r) > T_{\text{age}}$ , we may obtain the averaged color index within a given galactic projected radius  $R$ . We find for case (ii) that the averaged blueing within  $R < 0.1''$  due to collisions is not larger than 0.06 mag in  $\mu_U - \mu_V$  and 0.02 mag in  $\mu_V - \mu_I$ , and the averaged blueing within  $R < 0.05''$  due to collisions is not larger than 0.16 mag in  $\mu_U - \mu_V$  and 0.06 mag in  $\mu_V - \mu_I$ .

In Lauer et al. (1998), stellar collisions are claimed to be capable of causing observable blueing in the center of M32. However, Lauer et al. did not account carefully for distribution of stellar masses and radii, projection effects, and the difference between the color of BSs formed by stellar collisions and the original color of the center of M32.

Based on the above results for M32, we expect that stellar collisions cannot cause any observable color gradients at  $R > 0.1''$  in visible bands in the centers of M31 and other nearby galaxies. This result may be understood as follows: these systems have longer collision timescales than M32 (cf., Figure. 1b or Table 6 in Lauer et al. 1998); compared to the values obtained for M32, the factor  $|\Delta\mu_{\text{coll},m_{\text{tf}},C_1-C_2}^{\text{BS}}|$  (the difference between the color of BSs with mass  $m_{\text{tf}}$  and the original color of galactic centers) in equation (73) should not change significantly; and the ratios of the projection factors  $f_{\text{coll}}(R \ll r_b)/f_0(R \ll r_b)$  for core galaxies with small  $\gamma$  may become even smaller, and those for power-law galaxies do not significantly increase. Multicolor *HST* WFPC2 images show that the center of M31 appears bluer in a  $0.14'' \times 0.14''$  box than the rest of the nucleus and the surrounding bulge ( $1'' < R < 5''$ ), by  $\sim 0.1$  mag in  $\mu_V - \mu_I$  (see Table 2 in Lauer et al. 1998). Our estimate shows that the averaged blueing is not larger than 0.03 mag in  $\mu_V - \mu_I$  within  $R < 0.14''/2$  even for M32, and hence the  $\sim 0.1$  mag blueing in M31 is unlikely to be caused by stellar collisions. It is therefore worthwhile to investigate other mechanisms which may cause the blueing in the center of M31.

## 5 CONCLUSIONS

We have studied the effects of stellar collisions in realistic galactic centers, focusing on feeding massive BHs and color gradients.

We find that the mass involved in stellar collisions is not sufficient to provide the present BH mass in realistic galactic centers, especially in bright core galaxies. Similarly, Magorrian & Tremaine (1999) showed that stellar tidal disruption rates cannot contribute significantly to the present BH mass in galaxies brighter than  $\sim 10^9 L_\odot$ . These two results together discredit two proposed mechanisms (stellar collisions and tidal disruption of stars by central BHs, e.g., Frank 1978) for the growth of massive BHs in the centers in bright galaxies. The raw material for BH growth must therefore come from other sources, for example, the mass released by stellar evolution in the initial  $\sim 1$  Gyr of the galaxy's lifetime or gas that sinks to the galactic centers in a merger (see simulations on galaxy encounters in Barnes & Hernquist 1996). For both of the above mechanisms, massive BHs may form and grow rapidly, early in the history of the universe (e.g., at redshift  $z \sim 2-3$ , where galaxy encounters mostly occur in the hierarchical galaxy formation model). This scenario is consistent with the argument made by Yu & Tremaine (2002) that growth of high-mass BHs ( $> 10^8 M_\odot$ ) comes mainly from accretion during optically bright QSO phases (which is obtained by studying the relation between the local BH mass function and the QSO luminosity function).

We have analyzed how the color of a stellar system is affected by collisions of main-sequence stars. We account for the effects of collisions of main-sequence stars on color indexes at projected radius  $R$  due to three factors (see eq. 60): (i) the ratio of the change of luminosity density caused by stellar collisions to the original luminosity density of galactic centers at galactic radius  $r = R$ ; (ii) the difference between the colors of BSs and destroyed stars and the original color of galactic centers; and (iii) the projection effect between the surface brightness and the luminosity density. We find that collisions between main-sequence stars cannot cause observable color gradients in the visible bands at  $R > 0.1''$  in M32, M31 and other nearby galactic centers. This result is consistent with the lack of an observed color gradient in M32 at *HST* resolution. At even smaller radii, collisions between main-sequence stars are likely to cause the color difference larger than  $> 0.02$  mag (e.g., at most 0.08 mag at  $R = 0.02''$ ). The averaged blueing due to stellar collisions in the region  $R < 0.1''$  of M32 should not be larger than 0.06 mag

in  $\mu_U - \mu_V$  and 0.02 mag in  $\mu_V - \mu_I$ . The observed blueing in the center of the galaxy M31 (in a  $0.14'' \times 0.14''$  box; Lauer et al. 1998) must be caused by some mechanisms other than collisions between main-sequence stars.

This project was suggested by Scott Tremaine, my thesis advisor; and I am deeply indebted to him for his advice. I also thank Marc Freitag, Jeremy Goodman, Alison Sills and David Spergel for helpful discussions. Support for Proposal number HST-AR-09513.01-A was provided by NASA through a grant from the Space Telescope Science Institute, which is operated by the Association of Universities for Research in Astronomy, Incorporated, under NASA contract NAS5-26555. Support was also provided by NSF grant AST-9900316.

## REFERENCES

- Bailyn, C. D. 1995, *ARA&A*, 33, 133  
Bailey, V. C., & Davies, M. B. 1999, *MNRAS*, 308, 257  
Bailyn, C. D., & Pinsonneault, M. H. 1995, *ApJ*, 439, 705  
Barnes, J. E., & Hernquist, L. 1996, *ApJ*, 471, 115  
Benz, W., & Hills, J. G., 1987, *ApJ*, 323, 614  
Benz, W., & Hills, J. G., 1992, *ApJ*, 389, 546  
Binney, J., & Tremaine, S. 1987, *Galactic Dynamics* (Princeton: Princeton University Press)  
Byun, Y., et al. 1996, *AJ*, 111, 5  
del Burgo, C., Peletier, R. F., Vazdekis, A., Arribas, S., & Mediavilla, E. 2001, *MNRAS*, 321, 227  
Cole, A. A., et al. 1998, *ApJ*, 505, 230  
Corbin, M. R., O'Neil, E., & Rieke, M. J. 2001, *AJ*, 121, 2549  
Davidge, T. J., Rigaut, F., Chun, M., Brandner, W., Potter, D., Northcott, M., Graves, J. E. 2000, *ApJ*, 545, 89L  
Duncan, M. J., & Shapiro, S. L. 1983, *ApJ*, 268, 565  
Faber, S. M., et al. 1997, *AJ*, 114, 1771  
Frank, J. 1978, *MNRAS*, 184, 87  
Freitag, M., & Benz, W. 2001, *astro-ph/0101186*  
Freitag, M., & Benz, W. 2002, *A&A*, 394, 345  
Girardi, L., Bressan, A., Bertelli, G., & Chiosi, C. 2000, *A&AS*, 141, 371  
Kippenhahn, R., & Weigert, A. 1990, *Stellar structure and Evolution*, Springer-Verlag, Berlin  
Kroupa, P. 2002, *Science*, 295, 82  
Lai, D., Rasio, F. A., & Shapiro, S. L. 1993, *ApJ*, 412, 593  
Lauer, T. R., Faber, S. M., Ajhar, E. A., Grillmair, C. J., & Scowen, P. A. 1998, *AJ*, 116, 2263  
Leonard, P. J. T. 1989, *AJ*, 98, 217  
Magorrian, J., et al. 1998, *AJ*, 115, 2285  
Magorrian, J., & Tremaine, S. 1999, *MNRAS*, 309, 447  
Morris, M. 1993, *ApJ*, 408, 496  
Murphy, B. W., Cohn, H. N., & Durisen, R. H. 1991, *ApJ*, 370, 60  
Peletier, R. F. 1993, *A&A*, 271, 51  
Salpeter, E. E. 1955, *ApJ*, 121, 161  
Sills, A., Lombardi, J. C., Jr., Bailyn, C. D., Demarque, P., Rasio, F. A., & Shapiro, S. L. 1997, *ApJ*, 487, 290  
Sills, A., Faber, J. A., Lombardi, J. C., Jr., Rasio, F. A., & Warren, A. R. 2001, *ApJ*, 548, 323  
Stryker, L. L. 1993, *PASP*, 105, 1081  
Tremaine, S., et al. 1994, *AJ*, 107, 634  
Tremaine, S., et al. 2002, *ApJ* in press, *astro-ph/0203468*  
Vazdekis, A., Casuso, E., Peletier, R. F., & Beckman, J. E. 1996, 106, 307  
Verolme, E. K., Cappellari, M., Copin, Y., van der Marel, R. P., Bacon, R., Bureau, M., Davies, R. L., Miller, B. M., & de Zeeuw, P. T. 2002, *MNRAS*, 335, 517  
Yu, Q. 2002, *MNRAS*, 331, 935  
Yu, Q. & Tremaine, S. 2002, *MNRAS*, 335, 965

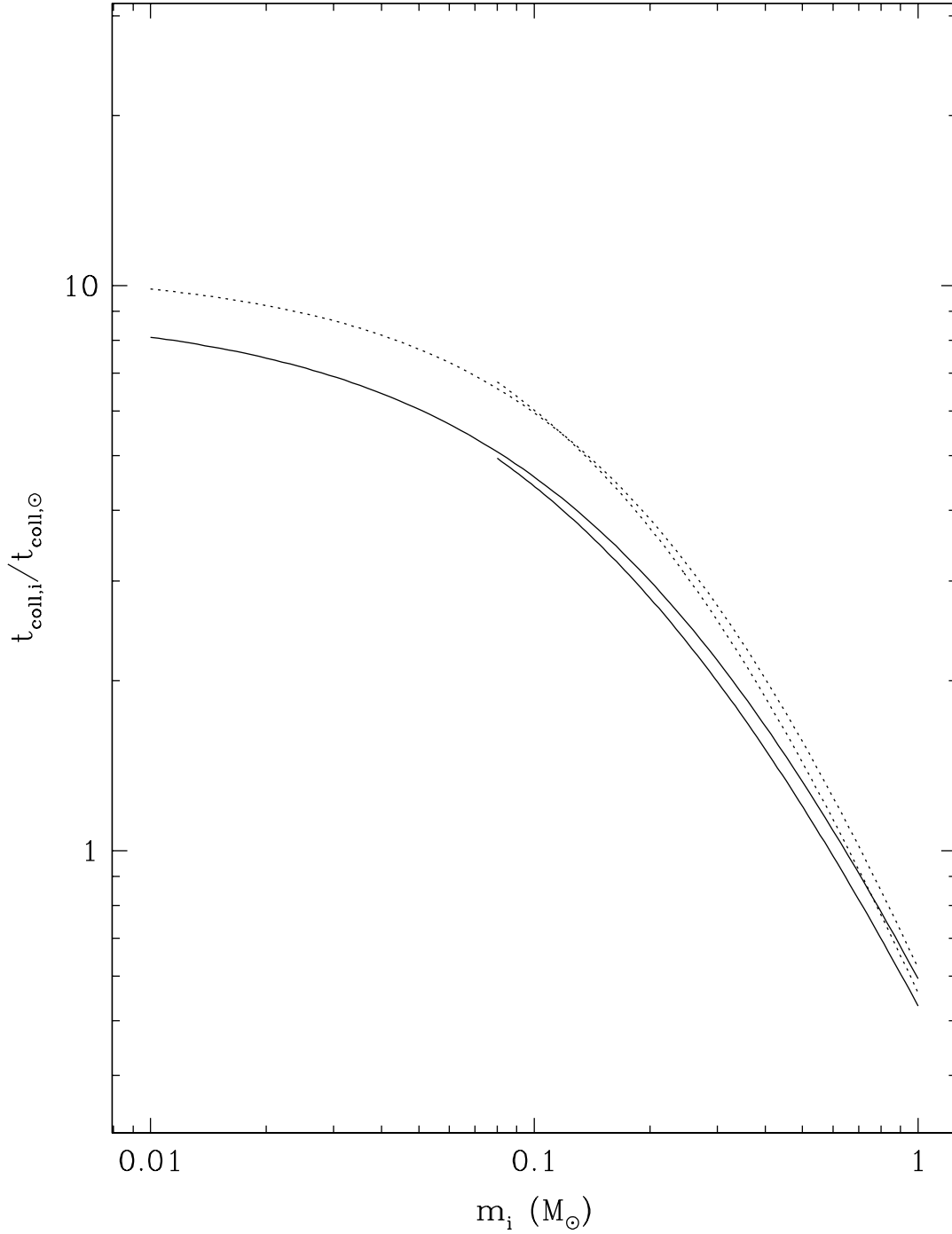


**Figure 4.** The ratio of collision timescales  $t_{\text{coll},i}/t_{\text{coll},\odot}$  as a function of stellar mass  $m_i$ . The quantity  $t_{\text{coll},i}$  (see eq. 5 or 31) is the collision timescale of stars with mass  $m_i$  obtained by assuming that the stellar system has a distribution of stellar masses and radii and ignoring collisions with post-main-sequence stars and stellar remnants; and  $t_{\text{coll},\odot}$  (see Fig. 1) is the collision timescale of stars by assuming that stars in the stellar system have solar mass and radius. Note that  $t_{\text{coll},i}$  at  $m_i = M_{\odot}$  is not necessarily equal to  $t_{\text{coll},\odot}$ . The dotted curves represent the results for  $\sigma(r) \ll v_{\text{esc},\odot}$ , and the solid curves represent the results for  $\sigma(r) \gg v_{\text{esc},\odot}$ . The curves ending at  $0.08 M_{\odot}$  are obtained by assuming the Salpeter IMF (eq. 26), and those ending at  $0.01 M_{\odot}$  are obtained by assuming the multi-power-law IMF (eq. 27). The turn-off stars are assumed to have a mass  $m_{\text{tf}} = 1 M_{\odot}$ .

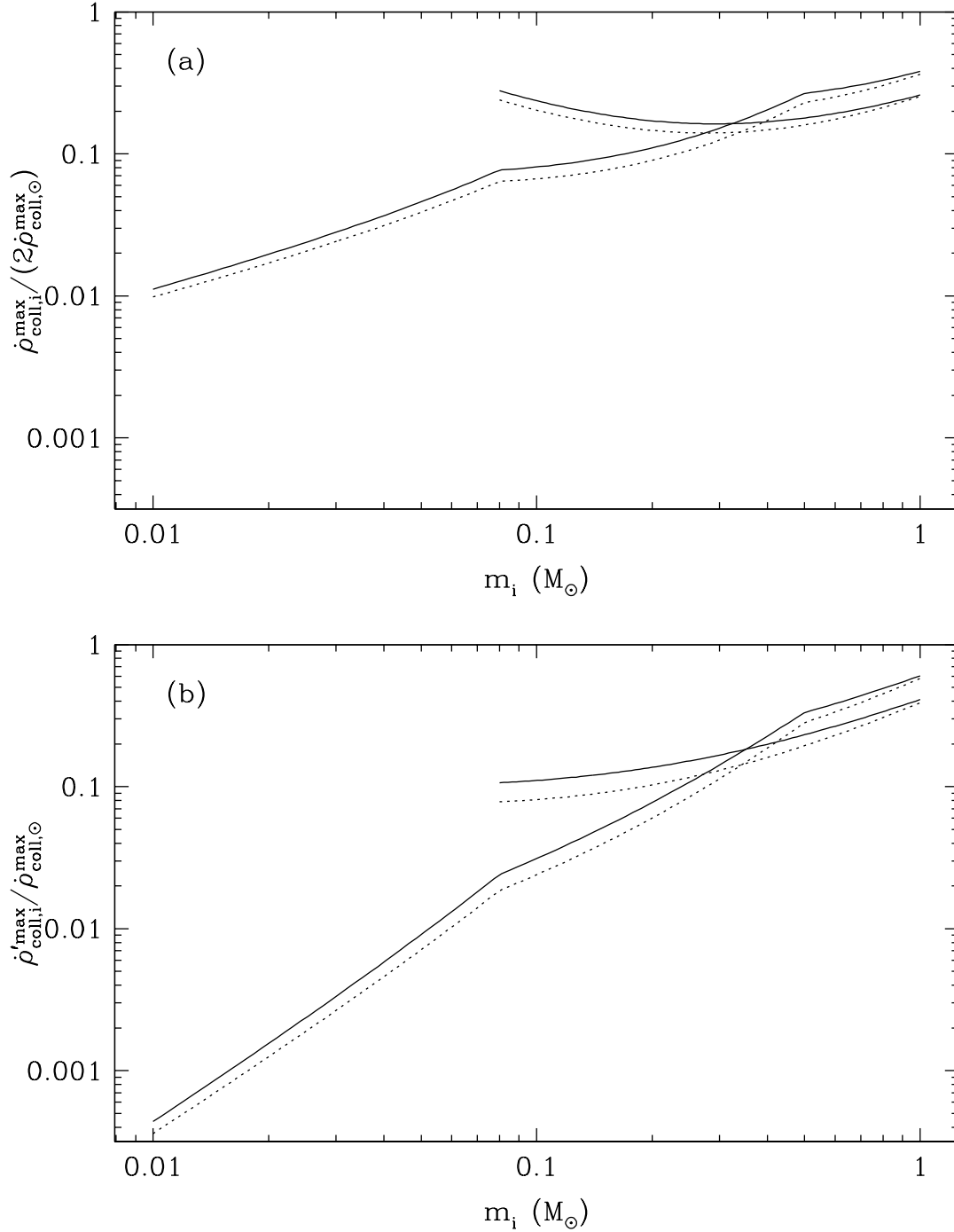


**Figure 5.** Panel(a): The ratio of  $\dot{\rho}_{\text{coll},i}^{\text{max}}/(2\dot{\rho}_{\text{coll},\odot}^{\text{max}})$  as a function of stellar mass  $m_i$  (cf., eqs. 32 and 33). Panel (b): The ratio of  $\dot{\rho}'_{\text{coll},i}^{\text{max}}/\dot{\rho}_{\text{coll},\odot}^{\text{max}}$  as a function of stellar mass  $m_i$  (cf., eqs. 34 and 35). The quantity  $\dot{\rho}_{\text{coll},i}^{\text{max}}d\ln m_i$  is the mass density of main-sequence stars involved in collisions with main-sequence stars with mass in the range  $\ln m_i \rightarrow \ln m_i + d\ln m_i$  per unit time; the quantity  $\dot{\rho}'_{\text{coll},i}^{\text{max}}d\ln m_i$  is the mass density of main-sequence stars with mass in the range  $\ln m_i \rightarrow \ln m_i + d\ln m_i$  involved in collisions per unit time; and the quantity  $\dot{\rho}_{\text{coll},\odot}^{\text{max}}$  is the mass density of main-sequence stars involved in collisions per unit time that is obtained by assuming that all the stars in the stellar system have solar mass and radius. The ratios  $\dot{\rho}_{\text{coll},i}^{\text{max}}/(2\dot{\rho}_{\text{coll},\odot}^{\text{max}})$  and  $\dot{\rho}'_{\text{coll},i}^{\text{max}}/\dot{\rho}_{\text{coll},\odot}^{\text{max}}$  are not necessarily 1 at  $m_i = M_{\odot}$ . The curves ending at  $0.08 M_{\odot}$  are obtained by assuming the Salpeter IMF (eq. 26) and those ending at  $0.01 M_{\odot}$  are obtained by assuming the multi-power-law IMF (eq. 27). The dotted curves represent the results for  $\sigma(r) \ll v_{\text{esc},\odot}$ , and the solid curves represent the results for  $\sigma(r) \gg v_{\text{esc},\odot}$ .

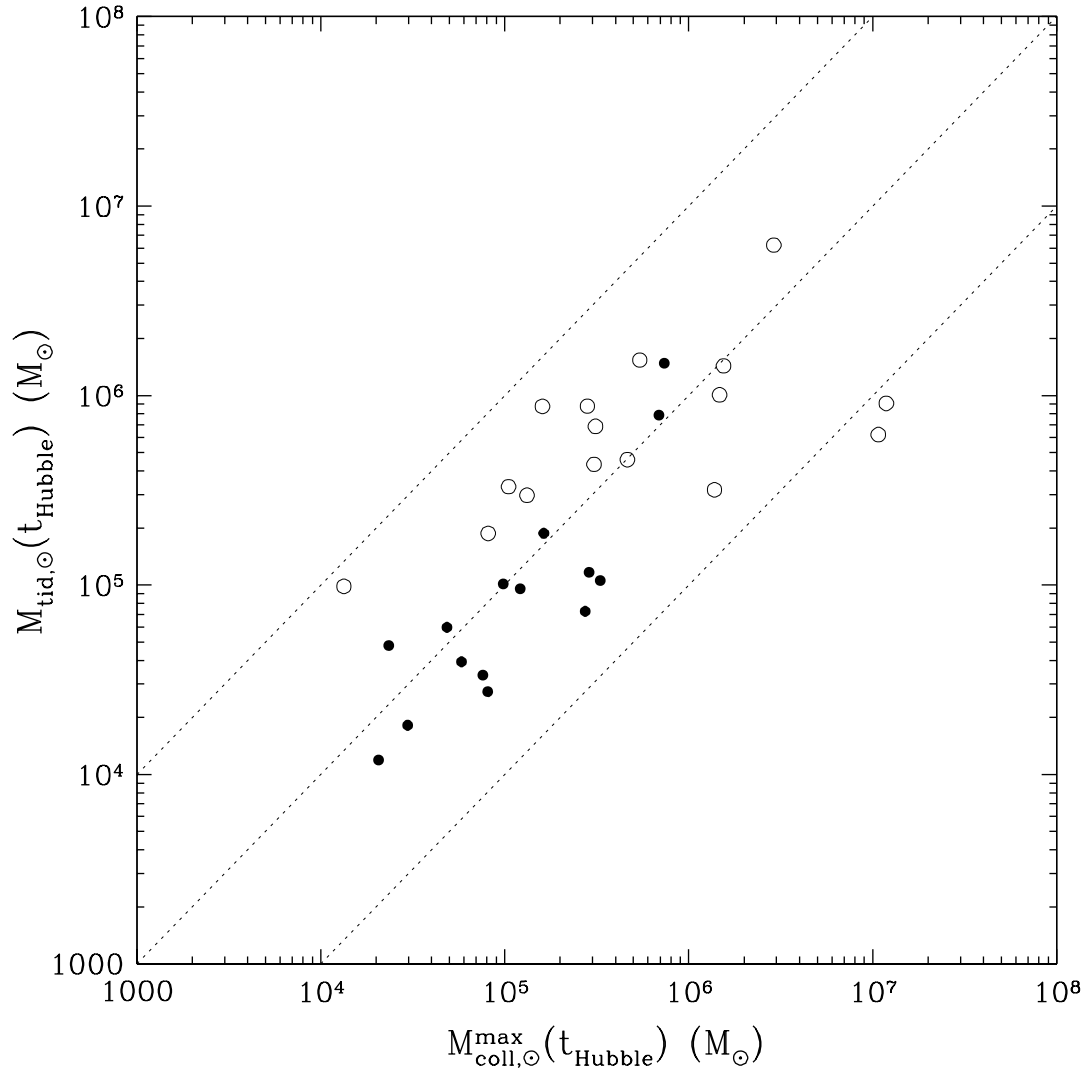


**Figure 6.** Stellar mass tidally disrupted or swallowed whole by central BHs  $M_{\text{tid},\odot}(t_{\text{Hubble}})$  versus stellar mass involved in collisions  $M_{\text{coll},\odot}^{\text{max}}(t_{\text{Hubble}})$  over a Hubble time (see Fig. 3a). All stars are assumed to have the solar mass and radius. Dotted lines are the reference lines for  $M_{\text{tid}}/M_{\text{coll}}^{\text{max}} = 0.1, 1, 10$ . Solid circles represent core galaxies and open circles represent power-law galaxies.  $M_{\text{tid},\odot}$  and  $M_{\text{coll},\odot}^{\text{max}}$  are generally comparable. See discussion in § 3.5.



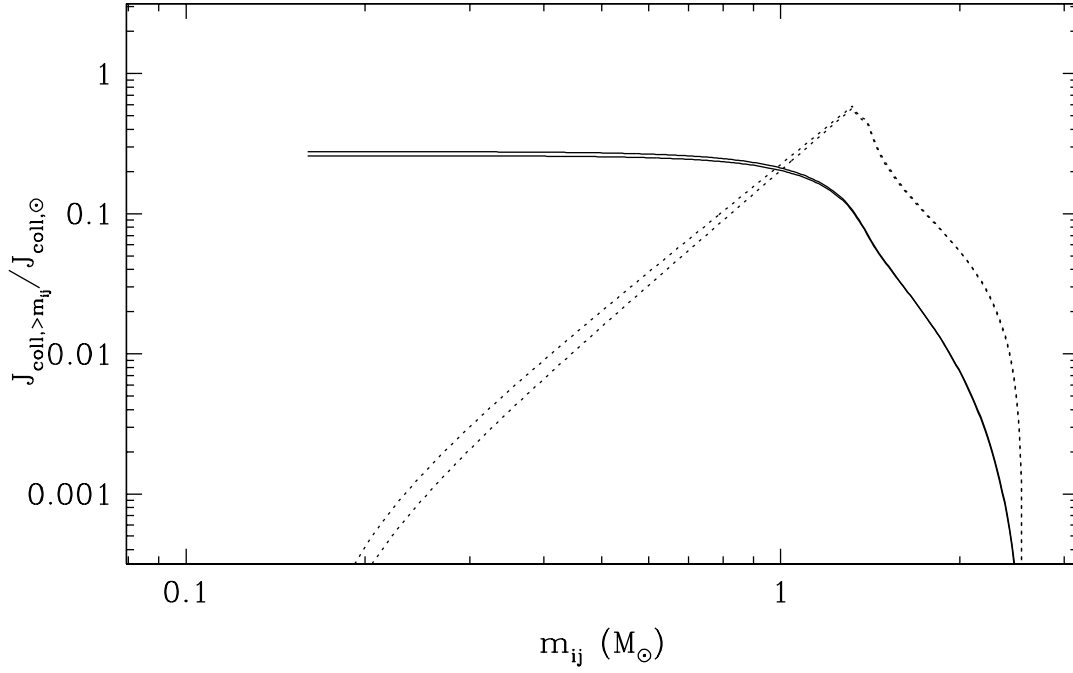


**Figure 7.** The ratio of the luminosity density contributed by BSs formed by collisions between main-sequence stars,  $J_{\text{coll},>m_{ij},C}^{\text{BS}}/J_{\text{coll},\odot,C}^{\text{BS}}$ , as a function of stellar mass  $m_{ij}$ , in M32 (solid lines for  $\sigma(r) \ll v_{\text{esc},\odot}$  or  $\sigma(r) \gg v_{\text{esc},\odot}$ , cf., eq. 65). The  $J_{\text{coll},>m_{ij},C}^{\text{BS}}$  represents the luminosity density contributed by BSs which are formed by collisions of two main-sequence stars with total mass higher than mass  $m_{ij}$ , and M32 is assumed to have a Salpeter IMF (eq. 26) and age  $T_{\text{age}} = 4 \times 10^9$  yr (see § 4.2.1). The  $J_{\text{coll},\odot,C}^{\text{BS}}$  represents the luminosity density contributed by BSs formed by collisions by assuming that the center of M32 is composed of identical stars with solar mass and radius. The dotted lines represent  $|dJ_{\text{coll},>m_{ij},C}^{\text{BS}}/d \ln m_{ij}|/J_{\text{coll},\odot,C}^{\text{BS}}$ ; and their peaks are located at  $m_{ij} \simeq m_{\text{tf}}$ , which shows that most of the surface brightness contributed by BSs comes from collisions between two stars with total mass around  $m_{\text{tf}}$ .

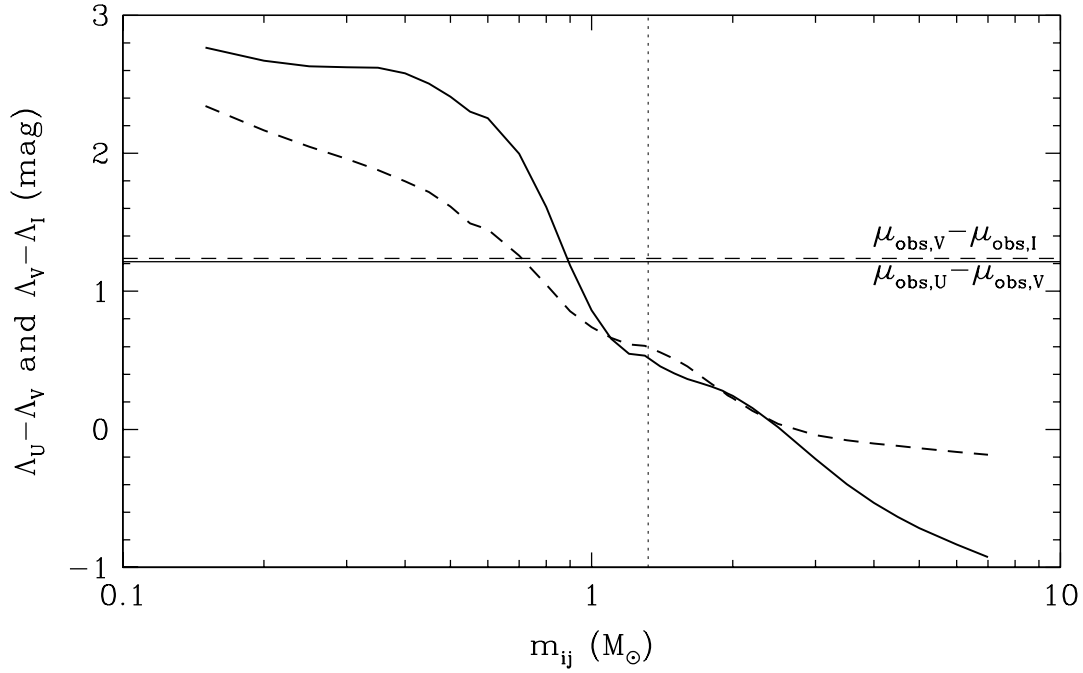


**Figure 8.** The color indexes  $\Lambda_U - \Lambda_V$  (thick solid line) and  $\Lambda_V - \Lambda_I$  (thick dashed line) of the time-integrated luminosity ( $\int_0^{T_{\text{age}}} L_C dt$ ) of stars during their main-sequence phases, as a function of stellar mass  $m_{ij}$  (eq. 68). The results are based on the stellar evolutionary tracks of Girardi et al. (2000). The stars have solar abundance. The horizontal lines give the observed color indexes,  $\mu_{\text{obs},U} - \mu_{\text{obs},V}$  (thin solid line) and  $\mu_{\text{obs},V} - \mu_{\text{obs},I}$  (thin dashed line) of the surface brightness of M32 at  $R = 1''$  (eqs. 54 and 55). The vertical dotted line represents stellar mass  $m_{ij} = 1.3 M_\odot$ , which is the turn-off mass at age  $T_{\text{age}} \simeq 4$  Gyr (see eq. 28).

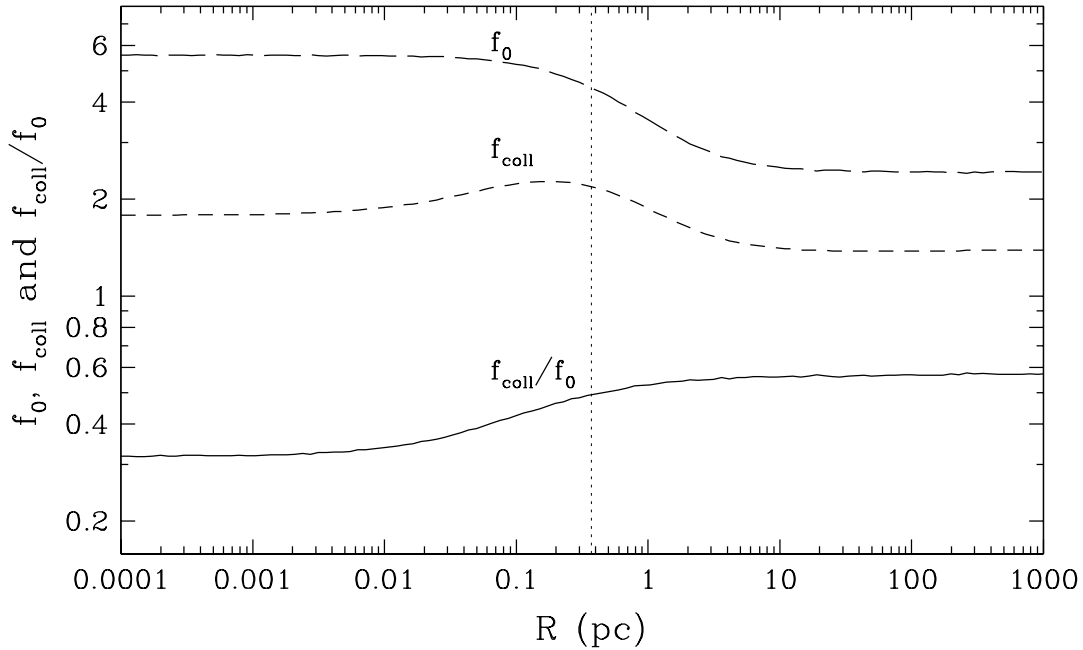


**Figure 9.** The projection factors  $f_0(R)$  (long dashed line),  $f_{\text{coll}}(R)$  (short dashed line) and their ratios  $f_{\text{coll}}(R)/f_0(R)$  (solid line) as a function of projected radius  $R$  in M32 (see eqs. 39 and 59). The vertical dotted line represents  $R = 0.1''$ . The results in the region not resolved by the *HST* ( $2R \lesssim 0.1''$ ) are obtained by extrapolating the Nuker-law-fitted surface brightness profile inwards.

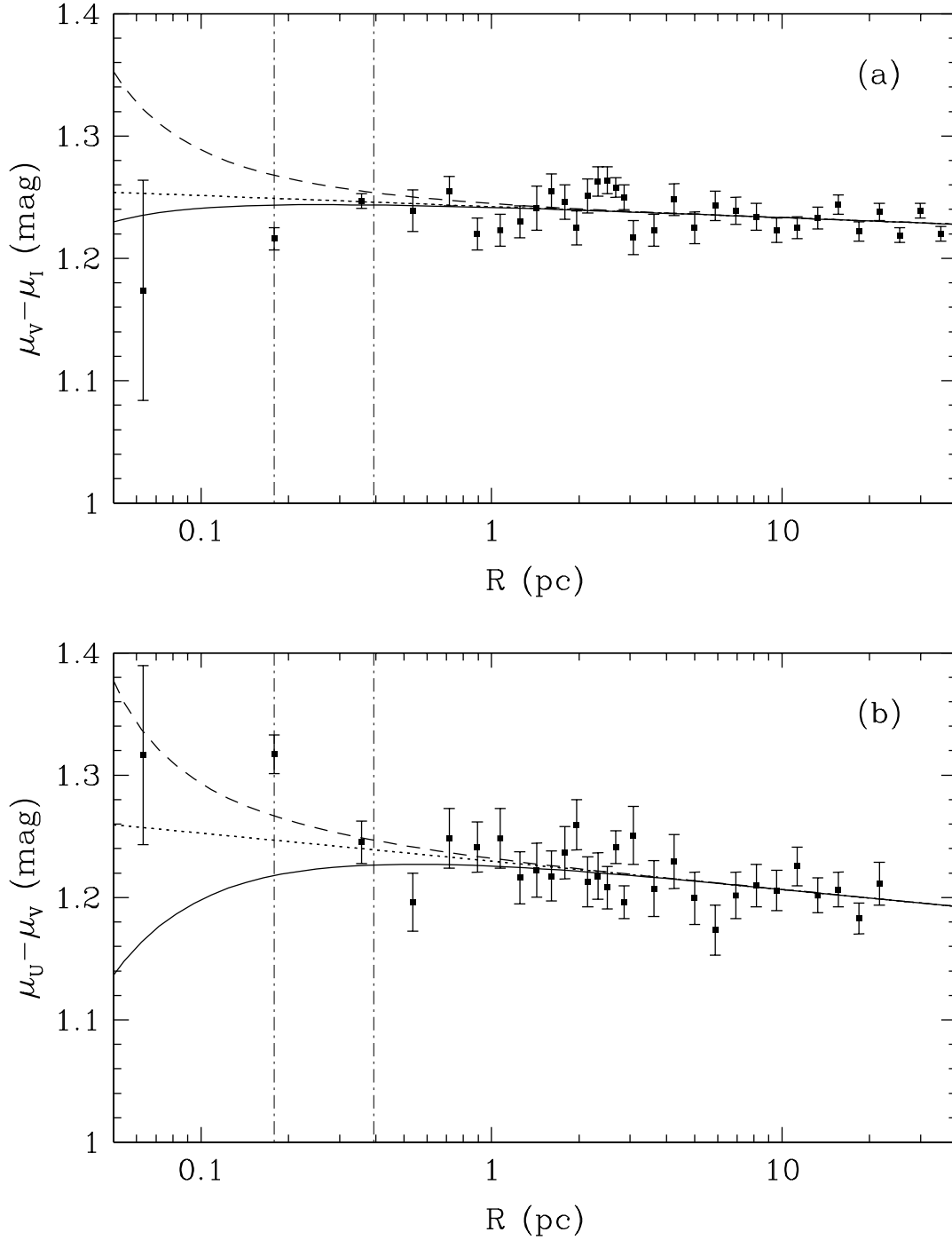


**Figure 10.** The estimated color indexes  $\mu_V - \mu_I$  and  $\mu_U - \mu_V$  (eq. 43) in the center of M32, as a function of projected radius  $R$ . Equations (36) and (40)–(45) are used in the calculation. The dashed lines represent the color gradients obtained by assuming that collisions always lead to destruction of both colliding stars and that no BSs are formed, [case (i) of § 4.1.1]; and the solid lines show the results obtained for case (ii), in which the colliding stars are assumed to form a BS with solar abundance. The left vertical dot-dashed line marks the  $HST$  resolution ( $R = 0.0455''$ ) and the right vertical dot-dashed line marks  $R = 0.1''$ . The solid squares are the color indexes obtained from observations (see Fig. 18 in Lauer et al. 1998); and the dotted lines represent a fit to the observed color index in the region  $0.1'' < R < 10''$  (eqs. 54 and 55), which is used as the initial state in our calculations (i.e.,  $\mu_{0,C_1} - \mu_{0,C_2}$  in eq. 40 and 45).